Received: 1 September 2020 | Accepted: 13 December 2020

DOI: 10.1111/gcb.15507

PRIMARY RESEARCH ARTICLE

Global Change Biology WILEY

Tundra wildfire triggers sustained lateral nutrient loss in Alaskan Arctic

Benjamin W. Abbott[1] | Adrian V. Rocha[2] | Arial Shogren[3] | Jay P. Zarnetske[3] | Frances Iannucci[4,5] | William B. Bowden[4] | Samuel P. Bratsman[1] | Leika Patch[1] | Rachel Watts[1] | Randy Fulweber[6] | Rebecca J. Frei[1,7] | Amanda M. Huebner[1] | Sarah M. Ludwig[8] | Gregory T. Carling[9] | Jonathan A. O'Donnell[10]

[1]Department of Plant and Wildlife Sciences, Brigham Young University, Provo, UT, USA

[2]Department of Biological Sciences & the Environmental Change Initiative, University of Notre Dame, Notre Dame, IN, USA

[3]Department of Earth and Environmental Sciences, Michigan State University, East Lansing, MI, USA

[4]Rubenstein School of Environment and Natural Resources, University of Vermont, Burlington, VT, USA

[5]Department of Biology and Wildlife, University of Alaska Fairbanks, Fairbanks, AK, USA

[6]Toolik GIS, University of Alaska Fairbanks, Fairbanks, AK, USA

[7]Department of Renewable Resources, University of Alberta, Edmonton, AB, Canada

[8]Department of Earth and Environmental Science, Columbia University, NY, NY, USA

[9]Department of Geological Sciences, Brigham Young University, Provo, UT, USA

[10]Arctic Network, National Park Service, Anchorage, AK, USA

Correspondence
Benjamin W. Abbott, Department of Plant and Wildlife Sciences, Brigham Young University, Provo, UT, USA.
Email: benabbott@byu.edu

Funding information
National Science Foundation, Grant/Award Number: 1026843, 1556772, 1906381, 1916565, 1916567 and 1916576

Abstract

Climate change is creating widespread ecosystem disturbance across the permafrost zone, including a rapid increase in the extent and severity of tundra wildfire. The expansion of this previously rare disturbance has unknown consequences for lateral nutrient flux from terrestrial to aquatic environments. Lateral loss of nutrients could reduce carbon uptake and slow recovery of already nutrient-limited tundra ecosystems. To investigate the effects of tundra wildfire on lateral nutrient export, we analyzed water chemistry in and around the 10-year-old Anaktuvuk River fire scar in northern Alaska. We collected water samples from 21 burned and 21 unburned watersheds during snowmelt, at peak growing season, and after plant senescence in 2017 and 2018. After a decade of ecosystem recovery, aboveground biomass had recovered in burned watersheds, but overall carbon and nitrogen remained ~20% lower, and the active layer remained ~10% deeper. Despite lower organic matter stocks, dissolved organic nutrients were substantially elevated in burned watersheds, with higher flow-weighted concentrations of organic carbon (25% higher), organic nitrogen (59% higher), organic phosphorus (65% higher), and organic sulfur (47% higher). Geochemical proxies indicated greater interaction with mineral soils in watersheds with surface subsidence, but optical analysis and isotopes suggested that recent plant growth, not mineral soil, was the main source of organic nutrients in burned watersheds. Burned and unburned watersheds had similar $\delta^{15}N\text{-}NO_3^-$, indicating that exported nitrogen was of preburn origin (i.e., not recently fixed). Lateral nitrogen flux from burned watersheds was 2- to 10-fold higher than rates of background nitrogen fixation and atmospheric deposition estimated in this area. These findings indicate that wildfire in Arctic tundra can destabilize nitrogen, phosphorus, and sulfur previously stored in permafrost via plant uptake and leaching. This plant-mediated nutrient loss could exacerbate terrestrial nutrient limitation after disturbance or serve as an important nutrient release mechanism during succession.

KEYWORDS
Arctic, disturbance, ecosystem succession, hydrology, nutrient flux, permafrost, streams, tundra, watershed, wildfire

 © 2021 John Wiley & Sons Ltd

1 | INTRODUCTION

Climate change is triggering widespread ecosystem disturbance across the permafrost zone (Abbott, Jones, et al., 2016; Biskaborn et al., 2019; Mack et al., 2011). Wildfire and permafrost degradation, which are the most common disturbance types in Boreal and Arctic ecosystems, respectively (Bond-Lamberty et al., 2007; Jones et al., 2015; Kim et al., 2020; Kokelj & Jorgenson, 2013), can mobilize organic matter and inorganic nutrients previously protected by cold and wet conditions (Abbott et al., 2015; Balshi et al., 2009; Rodríguez-Cardona et al., 2020; Walker et al., 2019). Whether nutrients liberated from thawing permafrost are available to terrestrial and aquatic primary producers will regulate key components of the Arctic carbon cycle and energy balance, including: the magnitude of carbon dioxide (CO_2) fertilization effects on net primary productivity (Balshi et al., 2009; McGuire et al., 2018); the rate and type of ecosystem recovery following disturbance (Chen et al., 2018; Kou et al., 2020; Pearce et al., 2014); the stability of soil organic matter (Craine et al., 2007; Mack et al., 2004); shifts in vegetation (Jiang, Rastetter, et al., 2015; Mack et al., 2008; Pearce et al., 2014); aquatic and marine primary productivity (Carey et al., 2019; Creed et al., 2018; McClelland et al., 2014; Wologo et al., 2020); and surface energy balance (Loranty et al., 2018; Rocha & Shaver, 2011b). Consequently, potential changes in nutrient availability are a major source of uncertainty in predicting net ecosystem carbon balance of the permafrost zone (Hoffman et al., 2017; Jiang et al., 2017; Jiang, Rocha, et al., 2015; McGuire et al., 2018; Shogren et al., 2020; Wright & Rocha, 2018).

Wildfire is already common in forest and some tundra ecosystems, where it structures the above and belowground carbon stocks and vegetation community (Balshi et al., 2009; Jones et al., 2013; Kim et al., 2020; Racine et al., 2004; Rocha & Shaver, 2011a). In Arctic tundra, wildfire is projected to increase 4- to 11-fold by 2100 due to increased temperature, evapotranspiration, ignition sources, and vegetation shifts (Abbott, Jones, et al., 2016; Hu et al., 2010, 2015). Because wildfire has been relatively rare in Arctic tundra in the past (Higuera et al., 2011; Jones et al., 2013; Rocha et al., 2012), it remains uncertain how changes in this key ecosystem disturbance will affect vertical (land-atmosphere) and lateral (land-water) nutrient fluxes (Larouche et al., 2015; Ludwig et al., 2018; Parham et al., 2013; Rodríguez-Cardona et al., 2020; Voigt et al., 2020).

Increased tundra wildfire could affect nutrient dynamics in several interrelated ways, depending on the timing and location of changes in nutrient supply and demand (Figure 1). On the supply side, wildfire can remove a substantial proportion of aboveground and belowground nutrients via combustion (Bret-Harte et al., 2013; Mack et al., 2011), decreasing organic nutrient sources and potentially lateral nutrient flux immediately postfire (Betts & Jones, 2009; Kawahigashi et al., 2011; Parham et al., 2013; Rodríguez-Cardona et al., 2020). However, the combustion of surface vegetation and peat decreases insulation and albedo, enhancing heat transfer into soils and deepening the seasonally thawed active layer (Holloway et al., 2020; Hu et al., 2015; Jiang et al., 2014; Jones et al., 2015; Loranty et al., 2018). This can allow water to flow through deeper soil horizons, which are often richer in solutes and inorganic nutrients, increasing nutrient supply (Frey & McClelland, 2009; Hewitt et al., 2015; Kawahigashi et al., 2011; Salmon et al., 2018). In areas of ice-rich permafrost, active layer thickening can trigger permafrost collapse and thermal erosion, known as thermokarst (Jones et al., 2015; Kokelj & Jorgenson, 2013; Larouche et al., 2015). Thermokarst releases above and belowground nutrients abruptly, temporarily increasing aquatic nutrient availability while decreasing terrestrial stocks (Abbott & Jones, 2015; Abbott et al., 2015; Buckeridge et al., 2016; Harms et al., 2014; Turetsky et al., 2019; Vonk et al., 2015). On the demand side, the combustion of vegetation could initially decrease terrestrial nutrient demand, followed by increased uptake during vegetation regrowth (Bret-Harte et al., 2013; Carey et al., 2019; Malone et al., 2018). Wildfire could also create temporal mismatches in nutrient supply and demand. For example, a deeper active layer or the development of taliks (layers of unfrozen soil beneath the active layer), which can be triggered by wildfire (Viereck et al., 2008; Yoshikawa et al., 2002), allows flow to persist through

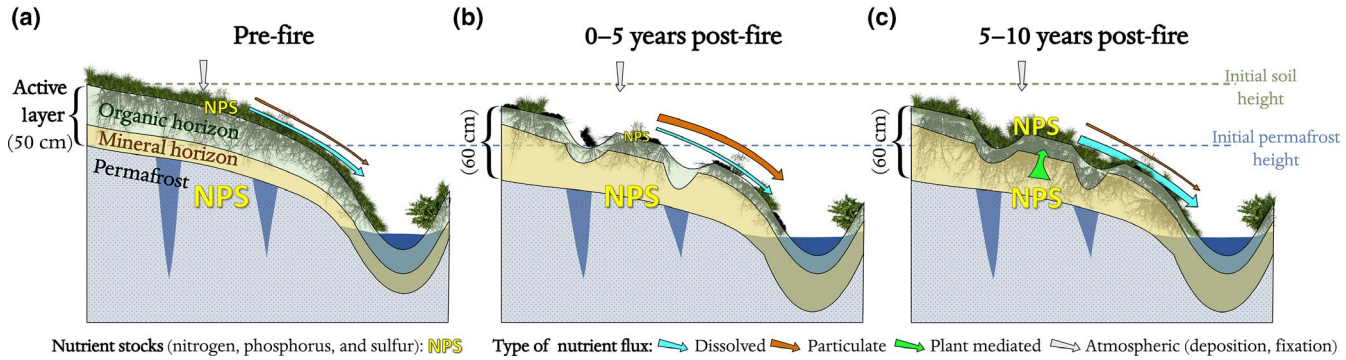


FIGURE 1 Conceptual diagram of wildfire effects on nutrient balance in Arctic tundra. (a) Predisturbance, there is low nutrient availability in the active layer because of limited decomposition and high demand from microorganisms and plants. There are large stores of nitrogen (N), phosphorus (P), and sulfur (S) in permafrost. (b) Combustion, thermo-erosion, and high demand from regrowth exacerbate nutrient limitation on land while increasing erosion and associated flux of particulate nutrients. (c) Regrowth stabilizes erosion while plants take up deeper nutrients, enhancing lateral flux of dissolved organic nutrients

a longer portion of the year, including after the end of the growing season when terrestrial nutrient demand decreases (Buckeridge & Grogan, 2010; Larouche et al., 2015; Rey et al., 2020; Shogren et al., 2020; Treat et al., 2016).

Finally, changes in vegetation driven by climate and disturbance could alter the timing and amount of terrestrial nutrient uptake and release. The stature and composition of plant communities is rapidly changing in high-latitude catchments (Carey et al., 2019; Myers-Smith et al., 2015; Sturm et al., 2001; Walker et al., 2006), and shifting plant communities could either increase or decrease lateral nutrient loss depending on the emerging community's nutrient acquisition strategies, such as nitrogen fixation, mycorrhizal association, and rooting depth (DeMarco et al., 2011; Högberg et al., 2010; Iwahana et al., 2016; Rhoades et al., 2001; Ruess et al., 2013). The net effect of these potential changes in nutrient supply and demand likely depends on local context, including soil organic matter stocks, permafrost stratigraphy, and hydrological conditions (Abbott et al., 2014; Jorgenson & Osterkamp, 2005; Loranty et al., 2016; Sturm et al., 2005; Tank et al., 2020; Zolkos & Tank, 2020). Given that initial and eventual effects of wildfire on lateral nutrient flux may be opposite (Figure 1), we need observations of tundra ecosystem response across temporal and spatial scales (Ludwig et al., 2018; Parham et al., 2013; Rodríguez-Cardona et al., 2020).

Quantifying nutrient dynamics at medium to large scales is challenging in any ecosystem (Bernhardt et al., 2017; Pinay et al., 2015), and particularly in permafrost regions where sites are remote and data are spatially and temporally sparse. This knowledge gap hinders process understanding of nutrient dynamics in complex permafrost landscapes (Hurrell et al., 2013; Kicklighter et al., 2013; Lawrence et al., 2011), and consequently our ability to predict the permafrost climate feedback (Abbott, Jones, et al., 2016; Chen et al., 2018; McGuire et al., 2018). One approach to quantify catchment-scale nutrient balance is to use streams as sensors of ecosystem processes (Brookshire et al., 2009; Carey et al., 2019; Shogren et al., 2019; Zarnetske et al., 2018). Stream nutrient concentrations and fluxes can indicate changes in terrestrial nutrient sources and sinks, providing a metric that integrates nutrient demand and uptake efficiency of terrestrial plants and microorganisms (Abbott et al., 2018; Frei et al., 2020; Wymore et al., 2019). This approach has been widely used to assess terrestrial elemental balance in non-permafrost ecosystems, generating fundamental insights into ecosystem succession and other processes over time (Fisher et al., 1998; Lovett et al., 2018; McClelland et al., 2007; Vitousek & Reiners, 1975). In high-latitude locations, this approach has been limited to a small number of watersheds (Kling & Kipphut, 2000; Malone et al., 2018; Metcalfe et al., 2018; Parham et al., 2013; Temnerud & Bishop, 2005), largely due to logistical limitations (but see Shogren et al., 2019).

In this context, we used an aerial sampling method to repeatedly measure stream chemistry in 42 tundra catchments in and around a large, 10 year old burn scar on the North Slope of Alaska (Jones et al., 2009; Mack et al., 2011). We hypothesized that there would be lower nutrient concentrations and fluxes in burned compared to unburned watersheds because of the loss of soil organic matter (Jiang, Rastetter, et al., 2015), rapid regrowth of vegetation (Bret-Harte et al., 2013), and recovering active layer thickness (Carey et al., 2019). We tested these hypotheses in a multi-proxy framework (Abbott, Baranov, et al., 2016; Frei et al., 2020; Shogren et al., 2019), using individual physicochemical parameters and relationships among multiple parameters in stream water to infer the hydrology and biogeochemistry of the burned and unburned tundra watersheds.

2 | METHODS

2.1 | The Anaktuvuk River fire

The study area is located on the North Slope of Alaska (Figure 2), 150 km south of the Arctic Ocean and ~90 km northwest of the Toolik Field Station, associated with the Arctic Long-term Ecological Research (LTER) site. The area is underlain by continuous permafrost and has a mean annual air temperature of −10°C, with mean monthly temperature ranging from −15°C in January to 12°C in July. Mean annual precipitation is ~320 mm, with roughly a third falling as snow (King et al., 2016; Toolik Environmental Data Center Team, 2019).

The Anaktuvuk River fire was ignited by a lightning strike in mid-July of 2007 (Liu et al., 2014). High air temperature, low precipitation, dry soils, and potentially site-specific characteristics allowed the fire to burn into early October (Jones et al., 2009; Liu et al., 2014). Eventually the fire burned 1039 km^2 of Arctic tundra bounded by the Nanushuk and Anaktuvuk Rivers on the west, and the Itkillik River on the east (Figure 2). The fire burned 80% of the area at moderate to extreme severities (Jones et al., 2009). On average, the fire removed one-third of the ~7,700 g C m^{-2} of organic matter and living biomass present before the burn (Mack et al., 2011), decreasing the organic-soil layer thickness from ~21 cm to ~15 cm (Liu et al., 2014; Mack et al., 2011; Rocha & Shaver, 2011b).

In the first 2 years after the fire, numerous thermokarst features formed, and the land surface subsided by an additional 2–8 cm compared to adjacent, unburned areas due to active layer thickening and thermokarst formation (Liu et al., 2014). In the 4 years following the fire, burned areas had active layer thickness that was 10 to 20 cm deeper than unburned areas (Rocha & Shaver, 2011b), though differences in active layer thickness between burned and unburned plots had decreased somewhat by our first sampling in 2017 (Carey et al., 2019). After 7 years (i.e., in 2014), thermokarst had affected 34% of the burn scar compared to only 1% of nearby unburned areas (Jones et al., 2015).

There are very few measurements of surface water chemistry or lateral flux from this area. However, in 2011 (4 years after the burn), stream chemistry was measured in four reference and six burned watersheds within or near the Anaktuvuk River fire scar (Larouche et al., 2015). The burned watersheds had higher dissolved organic carbon (DOC), ammonium (NH_4^+), phosphate (PO_4^{3-}), and total dissolved phosphorus and nitrogen than

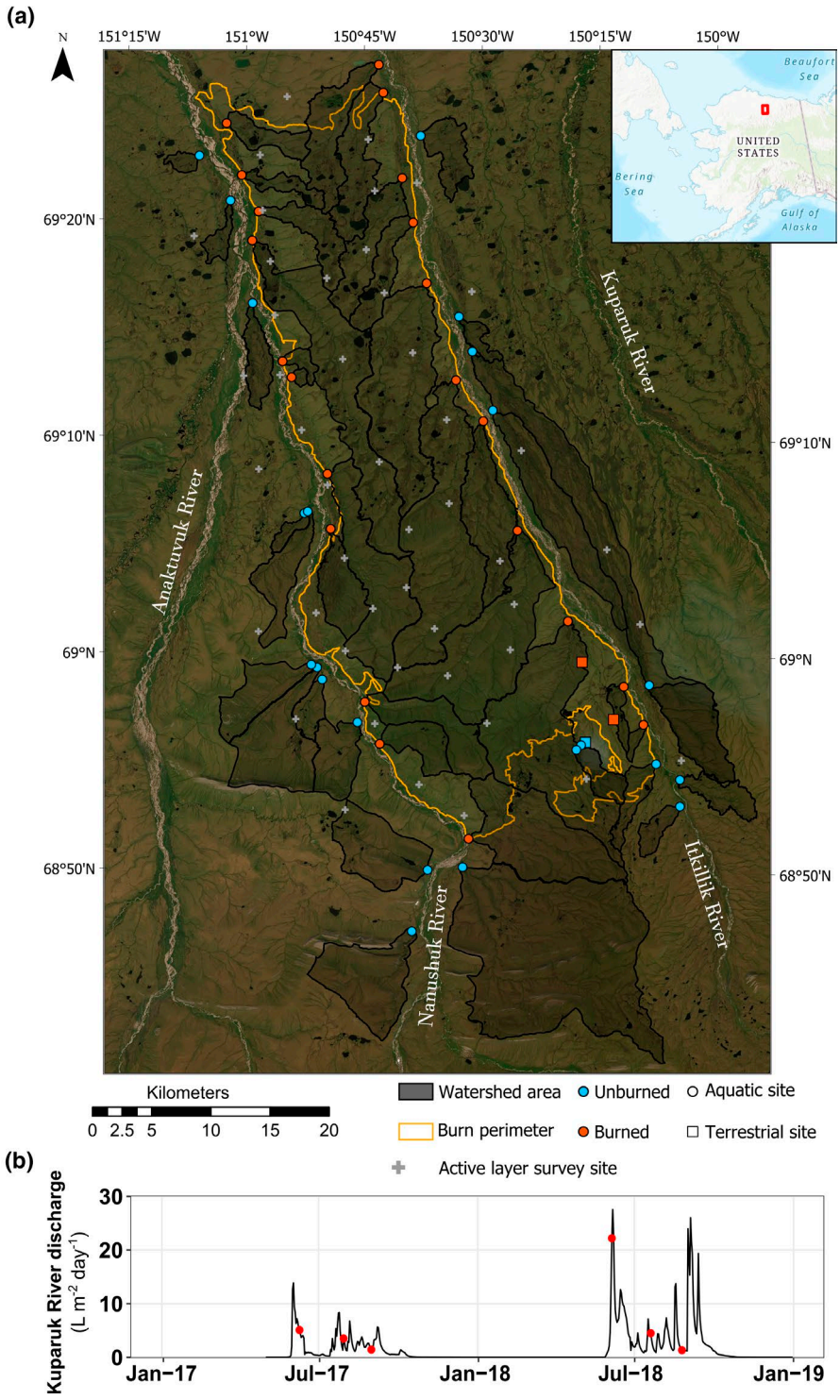


FIGURE 2 Map of the watersheds in and around the 2007 Anaktuvuk River wildfire (a), and hydrograph of the Kuparuk River (b). Stream samples were collected six times at the 42 watershed outlets (colored circles). Active layer depth and plant and soil C and N content were measured at the three terrestrial sites (colored squares). Active layer thickness was measured at 47 additional sites (gray crosses) in 2014 and 2019. Panel B shows specific discharge for the closest river with continuous flow data, with the sampling dates indicated by the red dots

unburned watersheds, but lower nitrate (NO_3^-) (Larouche et al., 2015).

The recovery of primary productivity occurred relatively quickly after the wildfire. Within 4 years, aboveground net primary productivity was equal in burned and unburned areas, though live biomass remained lower (Bret-Harte et al., 2013). However, the recovered plant community in the burn scar differs from unburned areas, with more deep-rooted gramminoids, especially tussock-forming cotton grass (*E. vaginatum*) and sedges (e.g., *C. bigolowii*), an absence of lichens, and a shift in non-vascular species (Bret-Harte et al., 2013; Carey et al., 2019; Jandt et al., 2012).

2.2 | Experimental design and stream sampling methods

We implemented a repeated synoptic sampling design, collecting water samples from many streams at multiple points in time (Abbott

et al., 2018; Dupas et al., 2019; McGuire et al., 2014; Shogren et al., 2019). Compared with more temporally intensive approaches that focus on a few locations, this spatially extensive design gave us more power to detect effects of the wildfire across different ecosystem gradients, though it reduced the breadth of parameters we could measure (e.g., no water discharge or in situ sensor measurements). This approach has proven effective at quantifying medium- to large-scale ecosystem characteristics in remote locations, including the Arctic (Abbott et al., 2015; Crump et al., 2012; Kling et al., 2000; Shogren et al., 2019). To compensate for a lack of directly measured covariates and ecosystem parameters for the sampling locations, we used a multi-proxy framework to constrain biogeochemical and hydrological processes based on water chemistry (Abbott, Baranov, et al., 2016; Kelleher et al., 2019; Pinay et al., 2015). For example, we inferred water flowpaths (depth of lateral flow relative to organic and mineral soil horizons) using ion concentrations and ratios (Barker et al., 2014; Keller et al., 2010), partitioning between evapotranspiration and lateral flow using stable isotopes in water (Berry et al., 2018; Bush et al., 2017), and sources of organic matter and nutrients (e.g., prefire soil vs. postfire fixation) using optical properties of dissolved organic matter (DOM) and stable isotopes of carbon (C) and nitrogen (N; Abbott, Baranov, et al., 2016; Malone et al., 2018).

We sampled all major tributaries to the Anaktuvuk, Nanushuk, and Itkillik Rivers over a 110 km range (68.7° to 69.5°N) to control for variation in ecosystem characteristics, including elevation, latitude, topography, permafrost state, and watershed size (Figure 2). Our sample sites included 42 accessible tributaries (21 burned and 21 unburned) in and around the burn scar, with watersheds ranging from 0.04 to 195 km^2 (mean and median areas of 34 and 21 km^2). These watersheds together drained 86% of the burn scar (Figure 2). Burned and unburned watersheds tended to be smaller at the northern end of the sampling area because of the confluence of the Anaktuvuk and Nanushuk Rivers on the west side of the burn (Figure 2).

The large geographic range of the sites and distance from the field station meant that landing the helicopter at each site was not possible because of fuel constraints. Consequently, we developed an aerial sampling method dubbed the Dübdeegan Dangle Maneuver (DDM), where we sampled the stream or river directly from the helicopter (Figure S1). During the DDM, we press-fit a prewashed, wide-mouth, 125 ml plastic bottle (high density poly ethylene) into a weighted cup at the end of a 4 m foldable aluminum sampling pole that we constructed from a broken camping table. As the pilot approached the site, we extended the pole and inserted the bottle under the water surface before the rotor wash from the helicopter disturbed the water surface to avoid stirring up sediment (Figure S1 and Video S1). After 1 or 2 s of filling, the bottle was retracted, capped, and put into a cooler as the pilot navigated to the next site. This sampling method allowed us to fly the perimeter of the burn scar while collecting samples in 2–4 h.

We collected samples in June, July, and August of 2017 and 2018, capturing three distinct periods in Arctic phenology (Shogren et al., 2020). The June sampling occurred during the spring snowmelt period when river discharge was high, thaw depth was low, and primary productivity was very low. The July samples were collected during the peak growing season when discharge and thaw depth were moderate, and productivity was near its peak. The August sampling occurred after deciduous plant senescence when discharge was low, productivity was moderate, and thaw depth was greatest (Table 1; Figure 3c). We collected samples from most of the sites for each sampling date, except for August of 2017, when a snowstorm and associated static discharge through the DDM pole to the helicopter airframe only allowed us to sample 19 of the sites (sample sizes reported in Table 1).

2.3 | Water discharge and remotely sensed data

While no stream discharge stations exist within or near the burn scar, we measured continuous discharge in the Kuparuk River (68.636°, −149.39°) from mid-June to mid-September in 2017 and 2018. This location was 14 km from the nearest site and 118 km

TABLE 1 Dates and conditions for the six samplings

Date	Daily Q (L m^{-2} day^{-1})	Weekly Q (L m^{-2} day^{-1})	Monthly precip. (mm)	Daily air temp. (°C)[b]	Weekly air temp. (°C)	Monthly air temp. (°C)	Thaw depth, unburned (cm)	Thaw depth, burned (cm)	*n* burned	*n* unburned
9-Jun-17	5.09[a]	6.03[a]	5.0	1.75	2.57	8.03	9.5	11.9	21	15
30-Jul-17	3.51	2.30	108	10.5	13.3	12.6	37.5	44.1	21	21
31-Aug-17	1.44	2.02	103	−3.04	−1.03	5.65	53.1	63.6	8	11
5-Jun-18	22.2[a]	18.7[a]	38	4.76	4.06	4.85	7.0[c]	12.6[c]	21	21
20-Jul-18	4.50	4.05	115	6.63	9.50	10.3	34.4	40.8	21	21
25-Aug-18	1.33	1.51	129	3.41	4.05	4.21	49.7	56.3	21	21

[a]Data for these dates were inferred based on lower Kuparuk station.

[b]All air temperature data from a 3 m height at the Toolik Field Station.

[c]Thaw depths for this date were interpolated because there was more than a week difference between thaw depth measurements and aquatic sampling.

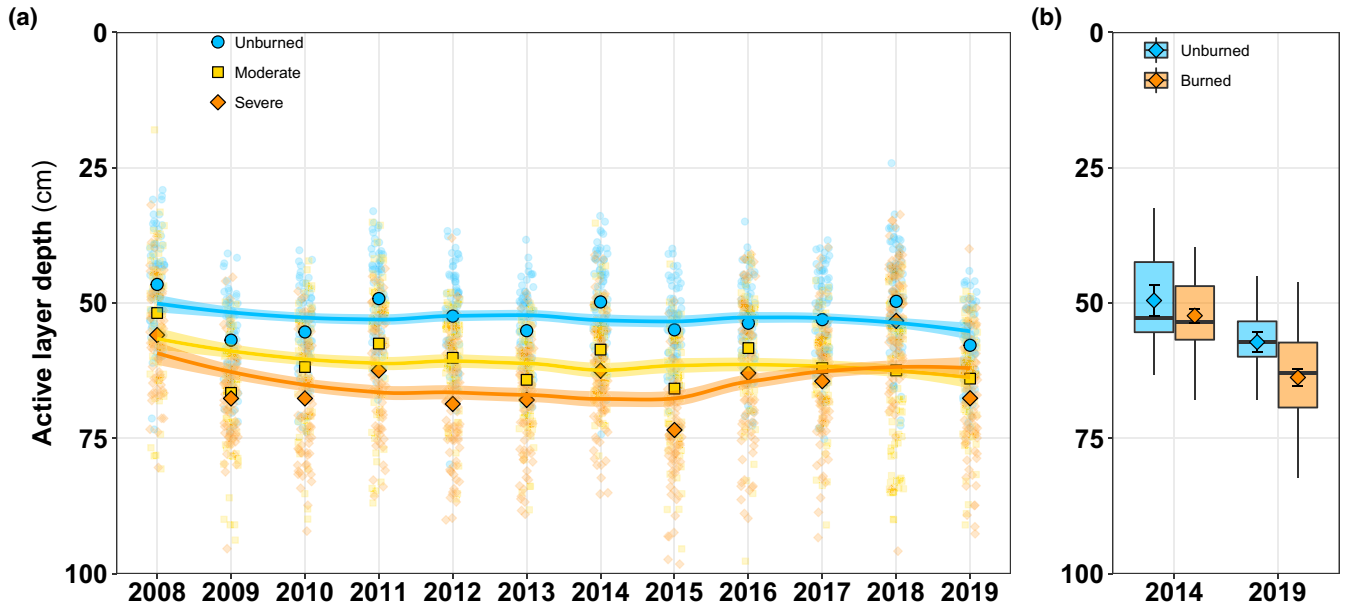


FIGURE 3 Active layer thickness (maximum seasonal depth of thaw) based on thaw-probe measurements. (a) Observations from the three terrestrial sites where active layer was measured yearly in late August or early September from 2008 to 2019. The outlined shapes represent the mean for that site and date, and the fitted lines show the smoothed conditional means and standard error across the period of observation. (b) Results of the active layer surveys done in 2014 and 2019 at 47 sites distributed within and near the burn scar (Figure 2). Box plots represent median, quartiles, 1.5 times the interquartile range (IQR), and points beyond 1.5 times the IQR. The diamonds and error bars represent the mean and standard error

from the most distant site. At the Kuparuk location, we manually measured discharge periodically using the velocity-area method with a flow meter (SonTek Flow Tracker), and we measured water depth (stage) every 15 min with an autonomous pressure transducer (Onset HOBO). We constructed a stage-discharge rating curve with these measurements, allowing estimation of continuous discharge across the flow season. To include the snowmelt period, when much of the annual discharge occurs, we completed the time series with data from the USGS Kuparuk River Station (15896000), approximately 100 km to the northeast of the burn scar. We calculated specific discharge (L m^{-2} day^{-1}) for each monitoring station and applied a linear conversion to the USGS data calculated during the period of overlap (i.e., mid-June to mid-September). While specific discharge could differ in and around the burn scar (King et al., 2018; Lyon et al., 2012), the relative magnitude of flow is likely similar, enabling calculation of flow-weighted means and estimates of lateral nutrient flux for the six samplings. We tested the assumption of similar specific discharge with water isotope measurements, which can indicate differences in evapotranspiration, storage, and runoff (Abbott, Baranov, et al., 2016).

To test our hypotheses about the relationship between catchment characteristics (e.g., size, burn severity, slope) and wildfire response, we delineated watersheds for each of the sampling locations using ArcGIS Pro (ESRI) with a 2 m resolution digital elevation model (DEM; Porter et al., 2018). We calculated elevation and slope directly from the DEM. We then intersected the watershed shapefiles with cloud-free Landsat and Sentinel images from before and after the burn to calculate several indices: the modified normalized difference water index (NDWI), normalized difference vegetation index (NDVI), and normalized burn ratio (dNBR; Boelman et al., 2011; Jones et al., 2009; Kolden & Rogan, 2013). We also calculated mean change in surface subsidence from 2006 to 2010 using published spatial data (Liu et al., 2014).

2.4 | Terrestrial plant and soil analyses

We quantified soil and plant C and N stocks in 2017 at an unburned, moderately burned, and severely burned site in or around the fire scar (Figure 2). Burn severity was previously determined for these sites, based on dNBR (Rocha & Shaver, 2011a). Following standard LTER protocols (Bret-Harte et al., 2013), vegetation harvests were used to determine above and belowground biomass for each species. Samples were collected at the end of July, during the peak growing season. At each site, vegetation and soils were sampled randomly at 10 m intervals along two 100 m transects. Within a 10 × 40 cm quadrat, the entire vegetation and organic soil layers (surface to mineral soil) were collected with a serrated bread knife and kept in plastic bags until processing. Upon arrival in the lab, quadrats were taken apart and plant material was sorted into aboveground leaf and woody biomass by species, and total belowground biomass. Leaf litter, coarse woody debris, and dead moss were also separated and measured. Samples were weighed after drying at 60°C for 3–4 days. A subset of dried samples (~5 per plant species part or horizon and site) were finely ground and analyzed for C (%) and N (%) using an elemental analyzer (Costech). We calculated site-level C and N content (g m^{-2}) using the area-weighted

values grouped by plant functional type: shrub, graminoid, lichen, and other (forbs, live moss, and unidentifiable).

To quantify soil C and N, we measured the depth of the peat and organic layer four times in each pit created by the biomass quadrat sampling. In half of the pits (i.e., 10), we extracted ~10 × 10 cm soil peat monoliths (i.e., "peat brownies"). Peat brownies were then wrapped in foil and transported to the lab, where they were dried and analyzed for C and N as previously described for the aboveground biomass. For each brownie, we separated the peat and upper and lower organic soil based on color and texture. The bulk density estimates (g cm^{-3}) were multiplied by the in-field measurements of horizon thickness (cm) and soil C and N content (%) to determine soil stocks (g m^{-2}).

At three of the terrestrial sites, thaw depth was measured monthly from 2008 to 2019 as described in Rocha and Shaver (2011b). Briefly, a metal rod was used to make 40 measurements in a 100 × 40 m permanent grid at each site with an additional 36 measurements randomly taken along four 30 m transects. Thaw depth was noted from the top of the moss layer or soil if moss was not present. We interpreted the last thaw depth measurement from each year (last week of August or first week of September) as the active-layer thickness (i.e., maximum annual thaw depth). Additionally, thaw depth was measured at 47 sites distributed within and near the burn scar in September 2014 and 2019 (Figure 2). At each of these survey sites, thaw depth was measured at 20 locations along a 20 m transect.

2.5 | Aqueous analyses

Upon returning to the lab, unfiltered water samples were immediately analyzed with a spectrophotometer (s::can, Austria) for UV-Vis absorbance (190–750 nm) and turbidity. We then filter-sterilized 60 ml of each sample with a prerinsed cellulose acetate membrane filter (0.2 µm pore size). Samples were refrigerated until analysis within 1 month. Filter-sterilized samples were analyzed for anions, cations, dissolved elements, water isotopes, C, and total dissolved N (TDN). We used ion chromatography (ThermoFisher Dionex) to quantify anions and cations, including fluoride (F^-), acetate ($C_2H_3O_2^-$), formate ($CH_2O_2^-$), chloride (Cl^-), nitrite (NO_2^-), bromide (Br^-), sulfate (SO_4^{2-}), PO_4^{3-}, lithium (Li^+), sodium (Na^+), potassium (K^+), magnesium (Mg^{2+}), and calcium (Ca^{2+}). NH_4^+ and NO_3^- were determined colorimetrically using an autoanalyzer (LACHAT). We summed NO_3^-, NO_2^-, and NH_4^+ to calculate dissolved inorganic N (DIN). We used an inductively coupled plasma optical emissions spectrometer (Thermo Scientific 7400 series) to quantify concentrations of dissolved elements (Al, As, B, Ba, Ca, Cd, Co, Cr, Cu, Fe, K, Mg, Mn, Mo, Na, Ni, P, Pb, S, Se, Si, Sr, Ti, V, and Zn). We replaced values that fell below the limit of detection (LOD) with the LOD/2. We measured DOC, dissolved inorganic C (DIC), and TDN on an elemental analyzer (Elementar, Germany) after evolution to CO_2 or NO. We used cavity ringdown spectroscopy (Los Gatos Research) to quantify stable isotope ratios of hydrogen (δD) and oxygen ($\delta^{18}O$) in water relative to Vienna Standard Mean Ocean Water (VSMOW). The analyzer had a precision of ±1 for δD and ±0.4 for $\delta^{18}O$. We calculated the local meteoric water line from published measurements of precipitation in the nearby Kuparuk River watershed (Harms & Godsey, 2017).

In 2018, we additionally froze a 30 ml subsample of 0.2 µm filtered water for stable isotope analysis of DOC and NO_3^- at the UC Davis Stable Isotope Facility. The $\delta^{13}C$ of DOC was quantified after digestion to CO_2 with an isotope ratio mass spectrometer (Sercon Ltd.). The $\delta^{15}N$ and $\delta^{18}O$ of NO_3^- were quantified via bacterial denitrification (Sigman et al., 2001), with the evolved N_2O measured on a mass spectrometer (Bremen).

We calculated dissolved organic N, phosphorus, and sulfur by difference between the total elemental amount and the inorganic solute (i.e., DON = TDN − DIN, DOP = P − PO_4^{3-}, and DOS = S − SO_4^{2-}). In addition to the individual solute concentrations, we calculated ratios of several geogenic solutes (Ca^{2+}, Mg^{2+}, Sr^{2+}, Na^+, SO_4^{2-}, and Ba^{2+}) that have been found in some regions to indicate depth of hydrological flow associated with seasonal and interannual changes in permafrost (Table S1; Keller et al., 2010, Lehn et al., 2017, Barker et al., 2014).

To calculate optical metrics of DOM composition (Table S1), we measured excitation emission matrices (EEMs) with a scanning fluorometer (Horiba). Scans were performed using a 150 watt Xenon lamp with varying integration times between 0.5 and 5 min depending on absorbance. Following standard methods (Cory et al., 2010), all samples were corrected for inner filter effects, Rayleigh scatter, and blank subtraction in MATLAB™ (version 6.9; MathWorks). We analyzed the EEMs to calculate several common indices of DOM composition, including biological index (BIX), humification index (HIX), fluorescence index (FI), E2/E3 index, and specific UV absorbance at 254 nm ($SUVA_{254}$; Fellman et al., 2010; Gabor et al., 2014, 2015; Kellerman et al., 2018; McKnight et al., 2001; Weishaar et al., 2003). The calculations and interpretations of these metrics are detailed in Table S1.

2.6 | Statistical analyses and calculations

We tested for relationships between water chemistry and catchment characteristics (including burn extent and severity) with Pearson correlation coefficients (*r*). Because the dataset included multiple measurements from the same sites, we calculated the site mean (flow-weighted and unweighted) for each parameter prior to calculating *r*. The flow-weighted values are more relevant to questions of mass balance (e.g., nutrient flux) because they mostly represent the high-flow sampling during snowmelt in June, while the unweighted values are more sensitive to changes throughout the year, including when flow was lower in July and August (Table 1). We calculated *r* for organic and inorganic nutrients, optical properties, stable isotopes, and geochemical ratios, using a decision criterion of $\alpha = 0.05$. Based on the high level of co-linearity observed among ions (see next paragraph), we calculated *r* for six representative solutes (Cl^-, Br^-, F^-, K^+, Mg^{2+}, Sr^{2+}) and the sum of anions and cations.

Because water chemistry parameters were often related in nonlinear ways, we calculated Spearman rank correlations (ρ) to quantify relationships among parameters (optical, chemical, and isotopic). Before calculating ρ, we scaled the data within sampling date (subtracting the mean and dividing by the standard deviation) to allow comparison of spatial differences among sites rather than temporal differences due to seasonality and discharge across the 2 years. Because of the larger number of comparisons, we used a decision criterion of $\alpha = 0.01$ when assessing statistical significance.

For each year (i.e., 2017 and 2018), we estimated annual organic nutrient flux from the unburned and burned area on an areal basis (mg m^{-2} $year^{-1}$). To do this, we first calculated the flow- and area-weighted mean concentrations for the entire burned and unburned watershed areas for each year. We then multiplied these concentrations by the cumulative specific discharge for that year (L m^{-2} $year^{-1}$). We recognize that these inferred discharge data are unlikely to provide high-precision estimates of flux (Lyon et al., 2012; Minaudo et al., 2017; Shogren et al., 2020). However, recent observations of the temporal persistence of spatial patterns in stream networks (Abbott et al., 2018; Shogren et al., 2019) and especially the high level of spatial replication in this study (Figure 2) suggest that relative comparisons among burned and unburned watersheds are robust.

We used analysis of variance (ANOVA) to test for differences in terrestrial stocks of C and N among the unburned, moderately burned, and severely burned sites. We considered the 20 sampling locations (10 for peat and SOM) from each site as the experimental unit. For post hoc comparisons, we applied a Bonferroni correction for a familywise α of 0.05. For the ANOVA and Pearson analyses, we visually inspected residual plots for deviations from normality, linearity, and homoscedasticity.

Statistical analyses and visualizations were performed in R (R Core Team, 2018; Wickham et al., 2020). The meteorological data are available from the Toolik Environmental Data Center (Toolik Environmental Data Center Team, 2019), and all chemistry and discharge data are attached.

3 | RESULTS

3.1 | Interannual variation and differences among catchments

The 2 years of the sampling were very distinct hydrologically and climatically (Figure 2; Table 1). Total specific discharge was 319 L m^{-2} $year^{-1}$ in 2017 and 702 L m^{-2} $year^{-1}$ in 2018. Specific discharge was higher in 2018 because of a larger snowmelt peak, large rain events in September, and more precipitation overall (236 mm in 2017 vs. 405 mm in 2018, June–September). The sampling dates captured most of this interannual and seasonal variability of flow, spanning 76% of the observed variation in river discharge across the sampling years (Figure 2b; Table 1). The flow season of 2017 was warmer than 2018, with a May–September mean air temperature of 5.3°C in 2017 and 4.0°C in 2018. At the unburned and severely burned terrestrial sites, active-layer thickness was shallower in 2018 than in 2017, though it was similar across years at the moderately burned site (Figure 3a).

The spatial analysis of watershed characteristics showed that burned and unburned watersheds were comparable for most topographic and surficial parameters (e.g., size, surface wetness, water coverage, location), though the slope and elevation happened to be slightly lower in burned watersheds, attributable to the geometry of the fire scar (Figure S2; Figure 2). Greenness (NDVI) based on satellite imagery from 2017 was similar for burned and unburned watersheds, indicating recovery of the aboveground plant community. As expected, burn severity (dNBR) based on satellite imagery from 2006 and 2008 was much higher in the burned watersheds, with a mean near 400 (severe burn) compared to 0 (no burn) for the unburned watersheds (Figure S2). The burned watersheds also showed substantial subsidence (mean of 3.9 cm in burned vs. 0 cm in unburned watersheds) based on data from 2010 (Liu et al., 2014). The burn parameters (i.e., burn extent, severity, and subsidence) were strongly correlated with each other ($r > 0.8$, $p < 0.001$; Table S2). Several of the watershed characteristics showed latitudinal gradients, with elevation, slope, and NDVI decreasing to the north, and the burn parameters and surface water increasing to the north, partially attributable to the latitudinal distribution of burned and unburned watersheds (Table S2).

Active layer thickness at the three terrestrial sites was greater at the burned locations across the 12 years of monitoring, with 2008–2019 means of 52.8 cm (±8.7; SD), 61.2 cm (±10.8), and 64.4 cm (±11.7) for the unburned, moderately burned, and severely burned sites, respectively (Figure 3a). Active layer thickness at the severely burned sites showed some signs of recovery, with depths converging toward the moderately burned values in 2016–2019 (Figure 3a). Conversely, there was greater active layer thickness and difference between burned and unburned locations in 2019 versus 2014, based on the thaw depth survey of 47 sites (Figure 3b).

3.2 | Terrestrial carbon and nitrogen stocks

Total ecosystem C and N to the mineral soil averaged 9800 g C m^{-2} (±910; SE) and 310 g N m^{-2} (±20) at the unburned site, 9300 g C m^{-2} (±910) and 200 g N m^{-2} (±22) at the moderately burned site, and 6800 g C m^{-2} (±950) and 250 g N m^{-2} (±24) at the severely burned site. Assuming similar preburn C and N, this represented mean C decreases of 5.7% and 31% for the moderately and severely burned sites, respectively, and mean N decreases of 34% and 18% relative to the unburned site (Figure 4a,b). Across all sites, belowground stocks (primarily peat and organic soil) accounted for an order of magnitude more C and N than aboveground stocks (Figure 4a,b). Aboveground biomass was similar across burn severities, indicating recovery of aboveground plant C and N, though the moderately burned site had less biomass (Figure 4a). Belowground biomass and soil C and N were generally lower at the burned sites, with 22%–85% less C and N than the unburned

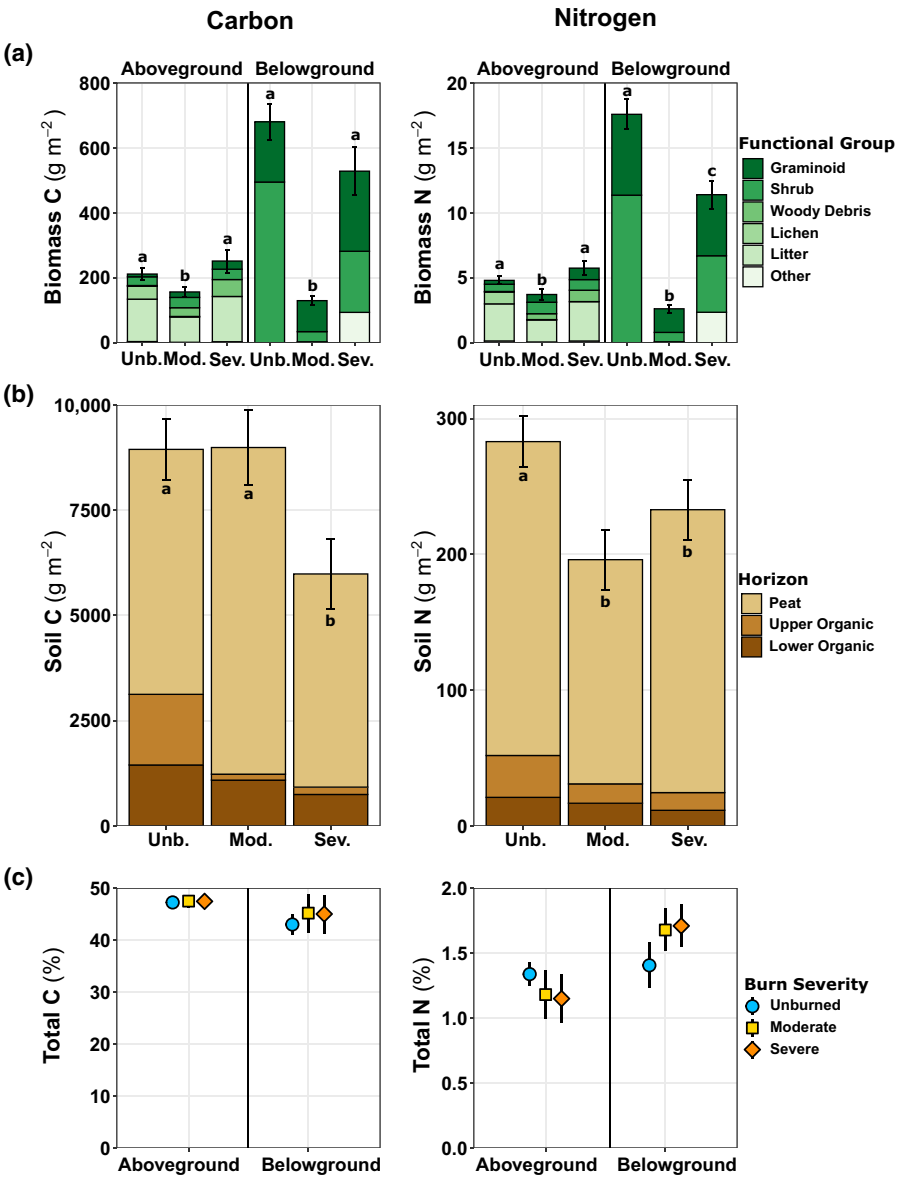


FIGURE 4 Plant biomass C and N content in biomass (a), peat and organic soil (b), and overall percent C and N (c). Bars and points represent the among-location mean and standard error, with letters indicating statistically significant differences. Data were collected in 2017 from the unburned, moderately burned, and severely burned sites in or near the fire scar (Figure 2)

sites (Figure 4a,b). The overall C and N percent was not significantly different across classes (Figure 4c). Graminoids made up a proportionally larger fraction of ecosystem C and N in both the moderately and severely burned sites (Figure 4a).

3.3 | Relationships between watershed characteristics and water chemistry

The unweighted and flow-weighted Pearson correlations among water chemistry and watershed characteristics were highly consistent for most parameters (Tables S3 and S4). Likewise, the Spearman correlations among parameters were highly consistent across burned and unburned watersheds (Figures S3 and S4). For simplicity, we hereafter refer to the unweighted means of the entire sample, except where specified otherwise.

The site means of all dissolved organic nutrients were positively correlated with burn severity (Figure 5a). Organic nutrients were also positively correlated with burn extent and subsidence, though not as strongly as with severity (Figure 6). There were several other correlations between specific organic nutrients and non-fire watershed characteristics (e.g., DOC with NDWI), but these relationships were weaker and largely attributable to the distribution of the fire scar across different landscape types. In contrast, none of the inorganic nutrients or isotopic parameters (i.e., isotopes of NO_3^-, DOC, and water) were correlated with the burn parameters, except dissolved silica (negatively correlated with extent and severity) and water isotopes (positively correlated with subsidence; Figures 5b and 6). Two of the six optical properties of DOM—$SUVA_{254}$ and FI—were correlated with the burn parameters, indicating a higher proportion of aromatic DOM and more plant versus microbial DOM sources in burned watersheds, respectively (Figure 5b). Optical properties were more correlated with nonburn parameters, particularly NDWI (Figure 6).

The sums of anions and cations were not correlated with burn extent or severity, but all ions were positively correlated with

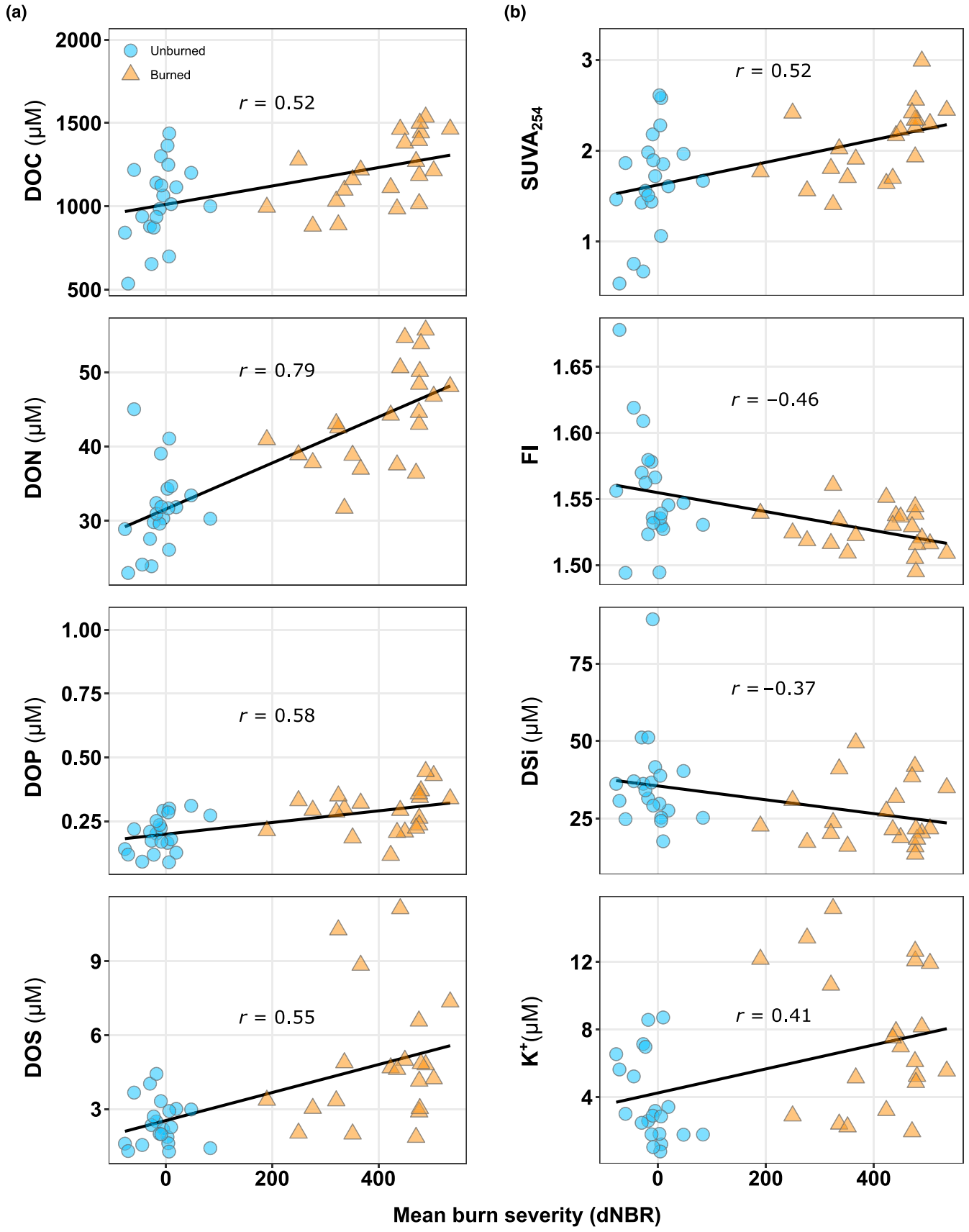


FIGURE 5 Significant Pearson correlations ($p < 0.05$) between burn severity and mean concentrations of (a) organic nutrients, and (b) optical properties, dissolved silica, and potassium for 21 burned and 21 unburned watersheds. For correlation coefficients and p-values for all chemical parameters, see Figure 6 and Tables S3 and S4

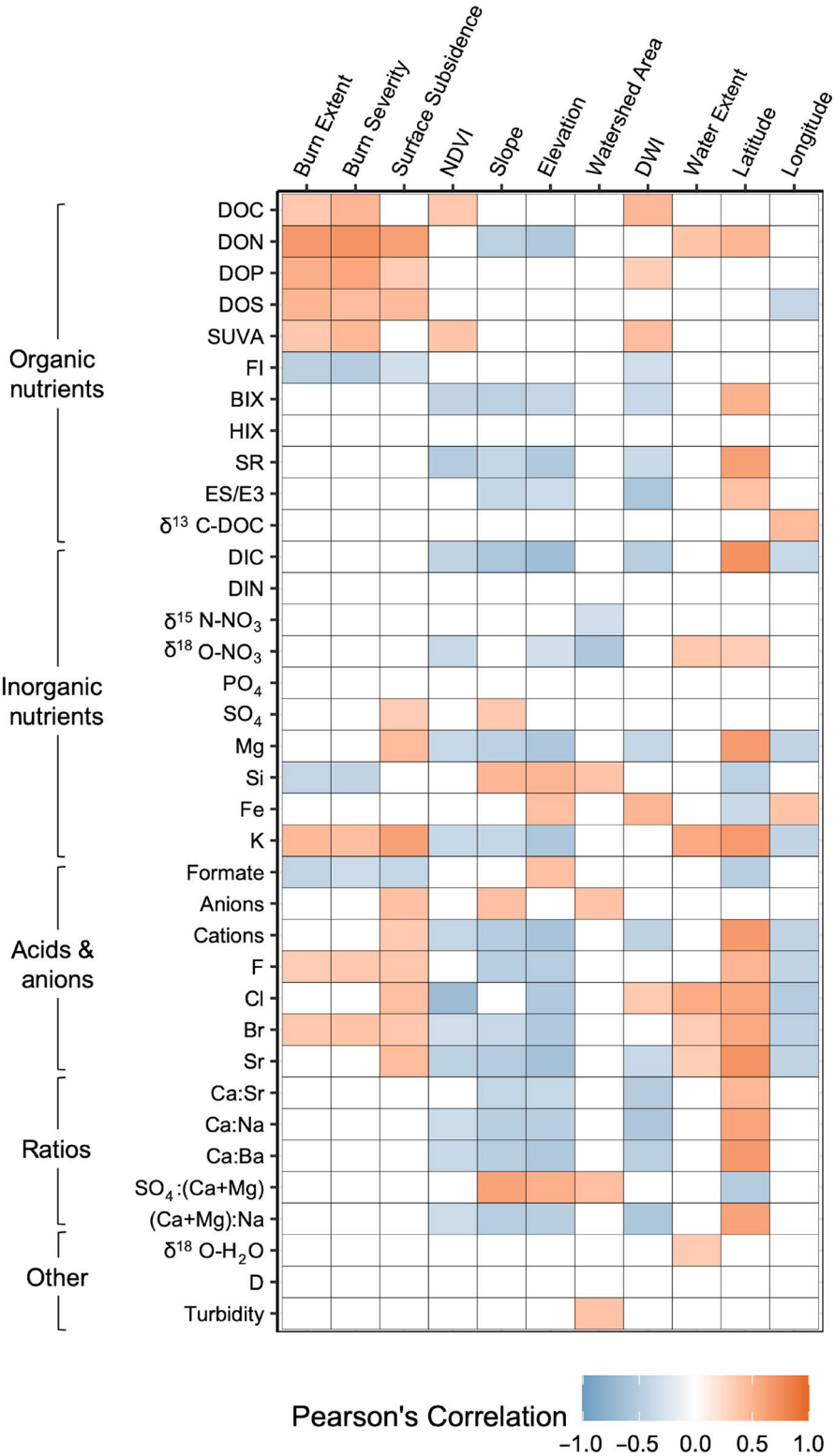


FIGURE 6 Correlation coefficients among catchment characteristics and mean water chemistry parameters. Only significant correlations ($p < 0.05$) are shown. For correlation coefficients and *p*-values for all parameters, see Tables S3 and S4

subsidence (Figure 6). Br^-, F^-, and K^+ were also positively correlated with burn extent and severity, though less than with subsidence. None of the geochemical ratios (e.g., Ca^{2+}:Sr^{2+}; Table S1) were correlated with the burn parameters (Figure 6). Most of the solutes and geochemical ratios showed significant negative correlations with elevation and slope, and consequently positive correlations with latitude (Figure 6; Table S2).

3.4 | Seasonal differences in water chemistry

For both burned and unburned watersheds, organic nutrient concentrations increased seasonally, with the largest increases between June and July, indicating a negative concentration-discharge relationship (Figure 7a). Inorganic nutrients did not show consistent seasonal patterns (Figure 7b). DIN and PO_4^{3-} concentrations were much lower than

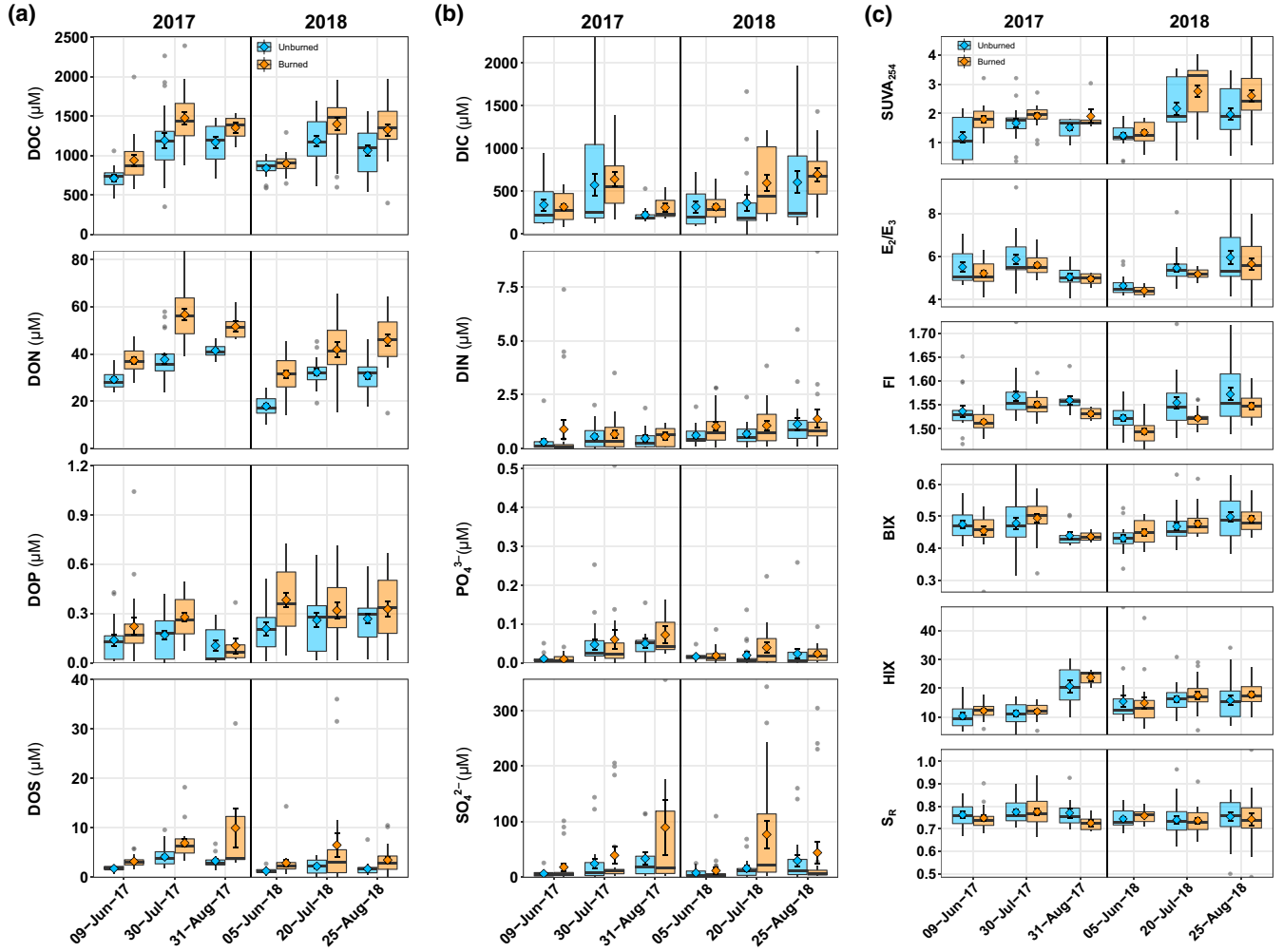


FIGURE 7 Seasonal concentrations of organic nutrients (a), inorganic nutrients (b), and optical properties of dissolved organic matter (c), in streams draining the burned (n = 21) and unburned (n = 21) watersheds. Symbology follows Figure 3b. For detailed interpretation of optical properties, see Table S1

their organic counterparts (i.e. DON and DOP), and DIC was somewhat lower than DOC (Figure 7b). However, SO_4^{2-} was much higher than DOS (Figure 7b). Inorganic nutrients were strongly left skewed (occasional extreme values), particularly PO_4^{3-} and SO_4^{2-} (Figure 7b).

The optical metrics of DOM properties showed various seasonal patterns (Figure 7c). The patterns were generally clearer in 2018, the wetter and cooler year (Table 1). $SUVA_{254}$ and FI, the two optical properties that varied with burn extent and severity (Figures 5 and 6), both showed seasonal increases, indicating a shift towards more aromatic and microbially modified DOM (Table S1). HIX also increased consistently in both years, indicating more degraded DOM with lower H:C ratios. The other parameters showed different patterns across years (E_2/E_3, BIX) or no change (S_R; Figure 7c).

Stable isotopes of DOC and NO_3^- did not show consistent trends through the season, except for $\delta^{18}O\text{-}NO_3^-$, which was substantially lower for both burned and unburned watersheds in the August sampling (Figure 8a). $\delta^{13}C$-DOC was not correlated with DOC concentration for burned or unburned watersheds (ρ = −0.16, p = 0.3; Figure 8b; Figure S3). The relationship between $\delta^{18}O$ and $\delta^{15}N$ of NO_3^- was consistent across burn status (ρ = 0.71, p < 0.01), suggesting similar sources and removal pathways of N (Figure 8b).

Water isotopes were strongly depleted ($\delta^{18}O$ < −15‰, δD < −120‰), consistent with the high latitude (Figure 9). Isotopic values showed strong seasonal increases, indicating a shift from snow- to rain-dominated runoff (Figure 9a). The seasonal increase was initially more rapid in the warmer, dryer year of 2017. However, the snow event on the week of the sampling in August resulted in substantially lower isotopic values, demonstrating the low storage and short hydrological residence times of these watersheds (Figure 9a). The local evaporation lines (relationship between $\delta^{18}O$ and δD in stream water) were consistent for unburned and burned watersheds (Figure 9b). Both lines plotted just below the local meteoric water line, suggesting limited evapotranspiration compared to runoff, supporting the assumption of similar specific discharge across burned and unburned watersheds.

Most of the ions showed increases through the season, except for K+, which showed a large pulse during snowmelt (June), and Cl^-, which was higher in the peak growing season (July) both years

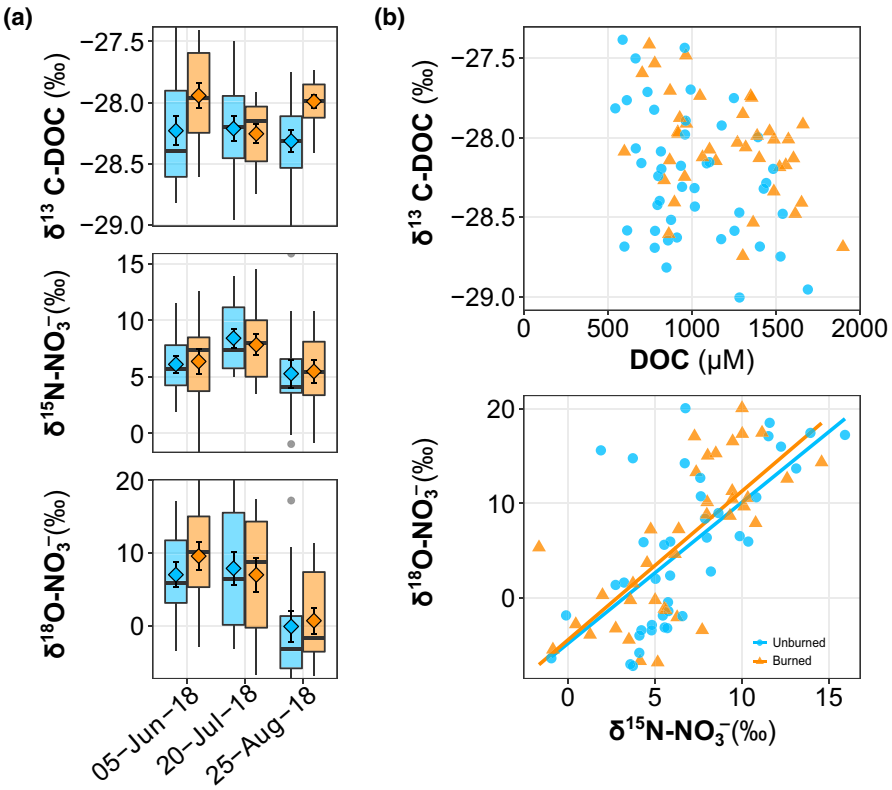


FIGURE 8 Stable isotopes of DOC and NO_3^-. (a) Seasonal changes in isotopic values for burned and unburned watersheds. Symbology follows Figure 3b. (b) Relationships of DOC concentration with $\delta^{13}C$ and NO_3^- isotopes

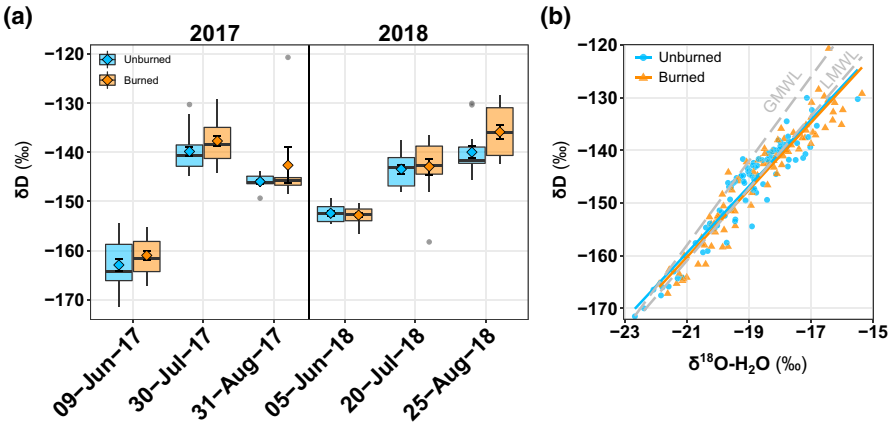


FIGURE 9 Seasonal variation in water isotopes (a) and the local evaporation lines between $\delta^{18}O$ and δD (b) in stream water. The global and local meteoric water lines are shown for reference (GMWL and LMWL, respectively). LMWL was calculated with precipitation measurements from the nearby Kuparuk River watershed (Harms & Godsey, 2017). Boxplot symbology follows Figure 3b

TABLE 2 Lateral flux (±SE) of organic nutrients from unburned and burned watersheds

Year	Q (L m^{-2} $year^{-1}$)	State	DOC (mg m^{-2} $year^{-1}$)	DON (mg m^{-2} $year^{-1}$)	DOP (mg m^{-2} $year^{-1}$)	DOS (mg m^{-2} $year^{-1}$)
2017	319	Unburned	3660 ± 190	151 ± 4.6	1.58 ± 0.21	39.1 ± 3.4
		Burned	4640 ± 273	211 ± 8.5	2.27 ± 0.43	54.1 ± 4.7
		Δ (%)	27.0	40.4	44.3	38.2
2018	702	Unburned	7310 ± 287	210 ± 16.7	5.19 ± 0.61	37.5 ± 4.6
		Burned	9050 ± 266	360 ± 17.8	8.90 ± 0.73	58.9 ± 13.5
		Δ (%)	23.8	71.7	71.6	56.9
Interannual mean		Unburned	5480 ± 256	180 ± 10.7	3.38 ± 0.41	38.3 ± 4.0
		Burned	6850 ± 268	286 ± 13.1	5.59 ± 0.58	56.5 ± 9.1
		Δ (%)	24.9	58.6	65.2	47.4

(Figure S5). As expected, the Ca^{2+}:Sr^{2+} ratio decreased systematically over the flow season, indicating deeper flow of water through the soil profile (Figure S5). However, the other ionic ratios potentially associated with thaw depth did not show consistent seasonal patterns (Figure S5).

3.5 | Lateral flux of organic nutrients

All organic nutrients showed substantially higher lateral flux in burned watersheds (Table 2). This was attributable to the significant correlations of organic nutrient concentrations with burn extent, severity, and subsidence (Figures 4 and 5; Tables S3 and S4). The interannual mean flux of DOC, DON, DOP, and DOS was 25 to 65% higher in burned watersheds compared to unburned watersheds (Table 2). For unburned and burned watersheds, organic nutrient fluxes were approximately twice as high in 2018 than 2017, due to greater runoff. Also, relative differences in organic nutrient flux between burn and unburned watersheds were greater for all nutrients except DOC in 2018 (Table 2).

4 | DISCUSSION

To investigate how tundra wildfire can affect lateral nutrient export, we quantified nutrient concentrations and a broad suite of water chemistry parameters from 42 watersheds in and around the >1000 km^2 Anaktuvuk River fire in northern Alaska. Contrary to our hypothesis that high terrestrial nutrient demand and lower C and N stocks would decrease lateral nutrient export, burned watersheds had substantially higher lateral flux of organic nutrients. Below, we discuss what could be causing these differences in lateral nutrient flux and what this nutrient loss might mean for tundra ecosystems recovering from wildfire.

4.1 | Evidence of persistent, plant-mediated export of permafrost nutrients

The observed lateral release of nutrients was unexpected on two accounts. First, this ecosystem is still recovering from a major disturbance that substantially decreased soil and biomass nutrient stocks (Bret-Harte et al., 2013; Jiang, Rastetter, et al., 2015; Mack et al., 2011). General theory and studies from this region predict strong net nutrient retention during this period of ecosystem recovery (Lovett et al., 2018; Malone et al., 2018; Pearce et al., 2014; Rastetter et al., 2020). Second, when lateral nutrient loss does occur in nutrient-limited permafrost ecosystems, it is usually due to temporal and spatial mismatches in supply and demand. For example, water flow below the rooting zone or outside of the growing season (i.e., shoulder seasons) can result in substantial nutrient loss from nutrient-limited permafrost regions (Jones et al., 2005, Treat et al., 2016, Harms & Jones, 2012, Shogren et al., 2020, Blume-Werry et al., 2016). However, these scenarios of deeper and longer flow predict lower organic to inorganic nutrient ratios, more processed DOM, higher solutes, and enriched stable isotope values for DOC and NO_3^- (Frey & McClelland, 2009; Harms & Jones, 2012; Keller et al., 2010; Lehn et al., 2017; MacLean et al., 1999; Malone et al., 2018; Mu et al., 2017; Shogren et al., 2020; Toohey et al., 2016; Treat et al., 2016; Wologo et al., 2020).

In every case, the patterns predicted by the deep flowpath and shoulder season hypotheses of nutrient flux were the opposite of what we observed. For example, the optical proxies and DOC isotopes suggested that the DOM and constituent organic nutrients are derived from postfire plant material in burned watersheds rather than directly from deeper organic matter activated by the wildfire (Figures 1 and 7). Likewise, the consistent differences in organic nutrient concentrations before, during, and after peak growing season, despite distinct soil nutrient dynamics (Buckeridge et al., 2013; Darrouzet-Nardi et al., 2019; McLaren et al., 2017; Melle et al., 2015), suggest that short-term terrestrial demand is not directly regulating lateral nutrient flux (Figure 7). Additionally, the isotopes of NO_3^- indicate that lateral N flux is not being driven by postfire N fixation (Malone et al., 2018). Finally, similar inorganic nutrient concentrations and the higher organic to inorganic nutrient ratios in burned watersheds suggests nutrient sourcing from organic horizons rather than mineral horizons. Regarding interpretation of nutrient patterns in streams, we point out that inorganic nutrient release from terrestrial environments could be obscured by uptake and mineralization in the aquatic environment, which is highly nutrient-limited (Kendrick et al., 2018; Kling & Kipphut, 2000; Rodríguez-Cardona et al., 2020), whereas organic nutrients move more conservatively through small Arctic watersheds such as these (Abbott, Baranov, et al., 2016; Shogren et al., 2019).

We hypothesize that the elevated organic nutrient flux from areas affected by the wildfire is caused by cumulative plant and mycorrhizal uptake of nutrients released from thawed permafrost (Figure 1). Rather than directly leaching nutrients from the thaw front, as predicted by the deep and shoulder season hypotheses, this plant-mediated hypothesis explains the sustained nutrient loss despite ecosystem succession, recovering active layer thickness, and intense terrestrial nutrient demand (Bret-Harte et al., 2013; Carey et al., 2019; Jiang, Rastetter, et al., 2015). Despite the loss of approximately four centuries worth of nutrients during the wildfire (Bret-Harte et al., 2013; Mack et al., 2011), over the first decade of postfire recovery, plants could have accessed nutrients released by thermokarst formation (i.e., subsidence; Jones et al., 2015; Liu et al., 2014) and increased active layer thickness (Carey et al., 2019; Rocha & Shaver, 2011b). The stronger and more consistent correlations between organic nutrients and burn severity versus subsidence (Figure 6) suggest that active layer thickening is more influential than thermokarst formation, though both processes are likely at play. Tundra plants—especially the deep-rooted graminoids more dominant in the burn scar (Figure 5)—readily take up nutrients released at the thaw front (Carey et al., 2019; Hewitt et al., 2015; Keuper et al., 2017; Salmon et al., 2018). For example, detailed characterization

of the plant community 4 years postfire showed lower C:N ratios in regrowth followed by greater allocation to belowground biomass (Bret-Harte et al., 2013). While we do not have detailed surface water data, measurements from the same time period suggest that enhanced lateral nutrient flux was already occurring 4 years postfire (Larouche et al., 2015). While the overall stocks of C and N are still lower in the burned watersheds (Figure 4), new growth from plants accessing thaw-front nutrients could be producing fresh organic matter that is more easily solubilized and leached, such as litter and fine roots (Neilson et al., 2018; O'Donnell, Aiken, Butler, et al., 2016; O'Donnell et al., 2013; Wickland et al., 2007, 2018; Zarnetske et al., 2018). Additionally, root exudates in the burned watersheds could be enhancing mineralization and potentially dissolution of peat and organic soil (Keuper et al., 2020), further fueling lateral loss of organic nutrients.

If this phenomenon of plant-mediated nutrient flux is widespread, it would explain the widely observed long-term increase in both DOM and solutes from most permafrost catchments where data are available (Drake et al., 2018; Frey & McClelland, 2009; Frey et al., 2007; Holmes et al., 2012; Kendrick et al., 2018; Mann et al., 2016; Tank et al., 2016; Toohey et al., 2016; Wauthy et al., 2018). The simultaneous increase in both DOM and solutes is contrary to the active layer thickening hypothesis, which predicts decreased DOM with permafrost degradation due to longer residence times and enhanced mineralization and sorption of DOM in mineral soil layers (Kicklighter et al., 2013; Laudon et al., 2013; MacLean et al., 1999; Mu et al., 2017; Striegl et al., 2005). Thermokarst formation, which delivers both DOM and solutes to river networks, has been proposed as one explanation to this paradox (Abbott et al., 2015; Bowden et al., 2012; Coch et al., 2019), but recent observations show that only some thermokarst features increase DOM delivery, likely based on local periglacial history and vertical distribution of organic matter (Tank et al., 2020; Zolkos & Tank, 2020). Additionally, most of the DOM in Arctic and Boreal surface waters is relatively modern (e.g., fixed within the last century), while thermokarst DOM is largely premodern (Burd et al., 2018; Ewing et al., 2015; Gaglioti et al., 2014; Mollenhauer et al., 2019; Raymond et al., 2007; Wang et al., 2018; Wild et al., 2019), further suggesting that recent plant growth is fueling increases in DOM flux from the permafrost region.

In addition to thermokarst formation, plant-mediated nutrient flux is a complementary hypothesis explaining the simultaneous increase in lateral DOM and solute flux. Areas undergoing active layer deepening could be losing solutes via deeper flow and thermokarst, while plant growth and regrowth fuel increasing lateral DOM flux. Solute and nutrient increases have primarily been attributed to deepening of the seasonally thawed active layer (Harms & Jones, 2012; Kawahigashi et al., 2006; Walvoord & Kurylyk, 2016), which allows water to move deeper in the soil profile where it interacts with solute-rich permafrost (O'Donnell, Aiken, Swanson, et al., 2016; Petrone et al., 2006; Reyes & Lougheed, 2015). The results from our study, however, suggest that surface subsidence is driving solute flux, while plant regrowth and nutrient mobilization from areas of deeper active layer are regulating organic nutrient flux. While these results are limited to a single region, they demonstrate the interactions between gradual and abrupt thaw, highlighting the need to simulate these processes together (Abbott et al., 2015; Turetsky et al., 2020).

4.2 | Implications of lateral nutrient loss for local ecosystems and global climate feedbacks

Our results reinforce evidence that permafrost degradation and wildfire can trigger substantial nutrient loss from ecosystems that are already nutrient-limited (Abbott et al., 2015; Betts & Jones, 2009; Mack et al., 2008; Pearce et al., 2014). Although we do not have complete budgets for most of the nutrients in this study, lateral N loss from burned watersheds is 2- to 10-fold higher than estimates of N fixation and atmospheric deposition for this region (Jiang et al., 2017; Mack et al., 2011; Weiss et al., 2005). In combination with vertical N losses that we did not quantify (e.g., denitrification and volatilization; Abbott & Jones, 2015; Malone et al., 2018; Voigt et al., 2020), our observations suggest that wildfire triggers a long-term and substantial nutrient deficit. This sustained loss could have contrasting consequences at global, regional, and local scales.

Starting at the global scale, predicting the permafrost C feedback to the Earth's climate depends on accurate estimates of greenhouse gas release and uptake in permafrost ecosystems (Schuur et al., 2015). Most Earth system models project substantial accumulation of C in living biomass and soil organic matter in the permafrost zone, sometimes sufficient to offset all greenhouse gas release from permafrost (i.e., a net stabilizing feedback from the permafrost zone; McGuire et al., 2018). However, most of these models are not fully coupled with nutrient cycles, and they often predict strong CO_2-fertilization effects and rapid ecosystem transitions (e.g., tundra to taiga), despite a lack of observations of these dynamics in current or past permafrost ecosystems (Abbott, Jones, et al., 2016; Fisher et al., 2019; Oberbauer et al., 1986; Wieder et al., 2015, 2019). If increased wildfire in Arctic tundra consistently increases lateral nutrient loss, the capacity of permafrost ecosystems to offset greenhouse gas release could be substantially diminished. Conversely, lower nutrient availability following wildfire could decrease N_2O production, reducing this non-carbon greenhouse gas (Voigt et al., 2020).

At the regional scale, sustained lateral flux of nutrients following wildfire could alter recipient ecosystems in aquatic, estuarine, and marine environments. The C balance and food webs of these ecosystems are highly sensitive to C, N, phosphorus, sulfur, and silica (Arrigo et al., 2012; Carey et al., 2019; Kendrick et al., 2018; McClelland et al., 2012; Slavik et al., 2004; Vancoppenolle et al., 2013), all of which were strongly affected by the wildfire in our study. The addition of bioavailable C and nutrients could affect C balance and light dynamics, potentially increasing or decreasing greenhouse gas release depending on interactions among organic matter production, breakdown, and environmental conditions (Wologo et al., 2020). Depending on the future extent of wildfire in areas of the

tundra biome where it has previously been rare (Abbott, Jones, et al., 2016; Jones et al., 2013; Rocha et al., 2012), plant-mediated nutrient loss could alter regional nutrient budgets, influencing C balance and habitat in donor and recipient ecosystems.

At the local scale, long-term nutrient deficits could slow encroachment of shrubs and forest into the tundra biome. Because the tundra-taiga transition is defined by nutrient status more than temperature, mechanisms that reduce nutrient availability effectively increase the resilience of tundra ecosystems to climate change (Bret-Harte et al., 2013; Wein & Bliss, 1973; Zimov et al., 2009). While tundra wildfire can trigger ecosystem transitions in areas that are warmer and more nutrient rich (Jandt et al., 2012; Landhausser & Wein, 1993), our study suggests that cold and nutrient-poor tundra areas may be resilient to forest encroachment and shrub expansion (Frost et al., 2013; Myers-Smith et al., 2011; Wein & Bliss, 1973; Zamin & Grogan, 2012), at least on decadal timescales. Postfire nutrient loss could be an important resilience mechanism—a way of shedding excess nutrients as permafrost degrades—similar to how conifer forests shunt nutrients during wildfire (Tierney et al., 2019). Alternatively or additionally, nutrient loss could convey adaptive advantages to the graminoids responsible for it, in this case primarily *E. vaginatum* (Bret-Harte et al., 2013; Mack et al., 2011; Wein & Bliss, 1973). *E. vaginatum* is already known to be an ecosystem engineer, lowering the temperature of underlying soil and permafrost by several degrees (Loranty et al., 2018; Shur & Jorgenson, 2007). If *E. vaginatum* is facilitating nutrient loss from burned tundra, it could be maintaining the oligotrophic nutrient conditions where it dominates tundra plant communities via nutrient shunting.

On a related topic, we emphasize that understanding the local to global impacts of permafrost wildfire on C dynamics requires better integration of hydrological processes into C and nutrient cycles (Douglas et al., 2020; Jorgenson et al., 2013; Lawrence et al., 2015; Neumann et al., 2019; Zarnetske et al., 2018). River runoff varied by more than a factor of two between the 2 years of our study, with the amount and type of lateral nutrient loss following suit (Table 2). This demonstrates how constraining the amount, timing, and flowpath of water through these ecosystems is crucial to determining local nutrient balance and ultimately, the global permafrost climate feedback (Laudon et al., 2013; Tank et al., 2020; Vonk et al., 2015).

4.3 | Wildfire effects on lateral flux depend on initial stocks and successional dynamics

While there are few studies of lateral nutrient flux following tundra wildfire, the available observations from other regions provide crucial context for our results (Larouche et al., 2015; Ludwig et al., 2018; Parham et al., 2013; Rodríguez-Cardona et al., 2020). Studies of Siberian tundra and taiga wildfires have found a more expected pattern of a pulse of inorganic nutrients, followed by the gradual recovery of organic nutrient concentrations over several decades (Parham et al., 2013; Rodríguez-Cardona et al., 2020). This aligns with terrestrial observations of relatively larger decreases in organic matter stocks in these areas (Ludwig et al., 2018) compared to what we observed on the North Slope. We suggest that this difference could be due to greater active layer thickness and lower initial C and nutrient stocks in ecosystems with much more frequent wildfires (Kirdyanov et al., 2020). The North Slope of Alaska has a very thin active layer and extremely infrequent wildfires, like much of the continuous permafrost zone (Jones et al., 2013; Rocha et al., 2012). These conditions could lead to greater postfire nutrient sources and enhanced importance of surface vegetation in driving lateral fluxes because the permafrost table largely constrains flow to the rooting zone (Neilson et al., 2018; Parham et al., 2013).

The importance of local ecological conditions in regulating the response to wildfire is further apparent in the geochemical data from our study. For example, only one of the several geochemical ratios that have been used as tracers of thaw depth in areas not far from the Anaktuvuk River fire (Barker et al., 2014; Keller et al., 2010; Lehn et al., 2017) showed the expected seasonal patterns (i.e., Ca^{2+}:Sr^{2+}; Figure S5). This should not be surprising given the heterogeneity of periglacial history and near-surface geology of the permafrost zone (Abbott et al., 2014; Larouche et al., 2015; Strauss et al., 2017; Tank et al., 2020). Considering this diversity of ecological context is crucial to accurate scaling and identification of robust trends. While it may still be premature, the superposition of global-scale soil and vegetation profiles with projected fire frequency (Hugelius, 2012; Kolden & Rogan, 2013; Olefeldt et al., 2016), could allow empirical and potentially mechanistic modeling of the effects of wildfire on lateral nutrient flux. In any case, considering differences in organic matter stocks, vegetation types, surficial geology, hydrology, and active layer thickness is crucial to projecting the response of C and nutrient dynamics to tundra wildfire across the permafrost zone.

ACKNOWLEDGEMENTS

This work was supported by the National Science Foundation award numbers 1916565, 1916567, 1916576, 1906381, DEB 1026843, and DEB 1556772. We thank the Toolik Field Station for world-class logistical support and the Toolik GIS Office for initial watershed delineation and analysis. We thank Natasha Griffith, Salvatore Curasi, Meghan Christie, Ian Klupar, Cameron MacKenzie, and Heidi Golden for dedicated and cheerful field and lab assistance. Rachel Buck and Andrew Luymes carried out the nutrient and ICP analyses in the BYU Environmental Analytical Laboratory. Kevin Rey performed the measurements of water isotopes at the BYU Geochemistry Lab. We thank Bianca Rodríguez-Cardona for input on an early version of the manuscript.

DATA AVAILABILITY STATEMENT

The data analyzed in this study are attached as supporting information.

ORCID

Benjamin W. Abbott https://orcid.org/0000-0001-5861-3481

Adrian V. Rocha https://orcid.org/0000-0002-4618-2407
Arial Shogren https://orcid.org/0000-0002-1284-3836
Jay P. Zarnetske https://orcid.org/0000-0001-7194-5245
Frances Iannucci https://orcid.org/0000-0002-7554-1819
Leika Patch https://orcid.org/0000-0001-5374-8256
Rachel Watts https://orcid.org/0000-0003-4595-5815
Randy Fulweber https://orcid.org/0000-0003-0537-4194
Sarah M. Ludwig https://orcid.org/0000-0002-2873-479X
Gregory T. Carling https://orcid.org/0000-0001-5820-125X
Jonathan A. O'Donnell https://orcid.org/0000-0001-7031-9808

REFERENCES

Abbott, B. W., Baranov, V., Mendoza-Lera, C., Nikolakopoulou, M., Harjung, A., Kolbe, T., Balasubramanian, M. N., Vaessen, T. N., Ciocca, F., Campeau, A., Wallin, M. B., Romeijn, P., Antonelli, M., Gonçalves, J., Datry, T., Laverman, A. M., de Dreuzy, J.-R., Hannah, D. M., Krause, S., … Pinay, G. (2016). Using multi-tracer inference to move beyond single-catchment ecohydrology. *Earth-Science Reviews*, *160*, 19–42.

Abbott, B. W., Gruau, G., Zarnetske, J. P., Moatar, F., Barbe, L., Thomas, Z., Fovet, O., Kolbe, T., Gu, S., Pierson-Wickmann, A.-C., Davy, P., & Pinay, G. (2018). Unexpected spatial stability of water chemistry in headwater stream networks. *Ecology Letters*, *21*, 296–308.

Abbott, B. W., & Jones, J. B. (2015). Permafrost collapse alters soil carbon stocks, respiration, CH_4, and N_2O in upland tundra. *Global Change Biology*, *21*, 4570–4587.

Abbott, B. W., Jones, J. B., Godsey, S. E., Larouche, J. R., & Bowden, W. B. (2015). Patterns and persistence of hydrologic carbon and nutrient export from collapsing upland permafrost. *Biogeosciences*, *12*, 3725–3740.

Abbott, B. W., Jones, J. B., Schuur, E. A. G., Chapin III, F. S., Bowden, W. B., Bret-Harte, M. S., Epstein, H. E., Flannigan, M. D., Harms, T. K., Hollingsworth, T. N., Mack, M. C., McGuire, A. D., Natali, S. M., Rocha, A. V., Tank, S. E., Turetsky, M. R., Vonk, J. E., Wickland, K. P., Aiken, G. R., … Zimov, S. (2016). Biomass offsets little or none of permafrost carbon release from soils, streams, and wildfire: An expert assessment. *Environmental Research Letters*, *11*, 034014.

Abbott, B. W., Larouche, J. R., Jones, J. B., Bowden, W. B., & Balser, A. W. (2014). Elevated dissolved organic carbon biodegradability from thawing and collapsing permafrost: Permafrost carbon biodegradability. *Journal of Geophysical Research Biogeosciences*, *119*, 2049–2063.

Arrigo, K. R., Perovich, D. K., Pickart, R. S., Brown, Z. W., van Dijken, G. L., Lowry, K. E., Mills, M. M., Palmer, M. A., Balch, W. M., Bahr, F., Bates, N. R., Benitez-Nelson, C., Bowler, B., Brownlee, E., Ehn, J. K., Frey, K. E., Garley, R., Laney, S. R., Lubelczyk, L., … Swift, J. H. (2012). Massive phytoplankton blooms under arctic sea ice. *Science*, *336*, 1408.

Balshi, M. S., Mcguire, A. D., Duffy, P., Flannigan, M., Kicklighter, D. W., & Melillo, J. (2009). Vulnerability of carbon storage in North American boreal forests to wildfires during the 21st century. *Global Change Biology*, *15*, 1491–1510.

Barker, A. J., Douglas, T. A., Jacobson, A. D., McClelland, J. W., Ilgen, A. G., Khosh, M. S., Lehn, G. O., & Trainor, T. P. (2014). Late season mobilization of trace metals in two small Alaskan arctic watersheds as a proxy for landscape scale permafrost active layer dynamics. *Chemical Geology*, *381*, 180–193.

Bernhardt, E. S., Blaszczak, J. R., Ficken, C. D., Fork, M. L., Kaiser, K. E., & Seybold, E. C. (2017). Control points in ecosystems: Moving beyond the hot spot hot moment concept. *Ecosystems*, *20*, 665–682.

Berry, Z. C., Evaristo, J., Moore, G., Poca, M., Steppe, K., Verrot, L., Asbjornsen, H., Borma, L. S., Bretfeld, M., Hervé-Fernández, P., Seyfried, M., Schwendenmann, L., Sinacore, K., Wispelaere, L. D., & McDonnell, J. (2018). The two water worlds hypothesis: Addressing multiple working hypotheses and proposing a way forward. *Ecohydrology*, *11*, e1843.

Betts, E. F., & Jones, J. B. (2009). Impact of wildfire on stream nutrient chemistry and ecosystem metabolism in boreal forest catchments of interior Alaska. *Arctic, Antarctic, and Alpine Research*, *41*, 407–417.

Biskaborn, B. K., Smith, S. L., Noetzli, J., Matthes, H., Vieira, G., Streletskiy, D. A., Schoeneich, P., Romanovsky, V. E., Lewkowicz, A. G., Abramov, A., Allard, M., Boike, J., Cable, W. L., Christiansen, H. H., Delaloye, R., Diekmann, B., Drozdov, D., Etzelmüller, B., Grosse, G., … Lantuit, H. (2019). Permafrost is warming at a global scale. *Nature Communications*, *10*, 264.

Blume-Werry, G., Wilson, S. D., Kreyling, J., & Milbau, A. (2016). The hidden season: Growing season is 50% longer below than above ground along an arctic elevation gradient. *New Phytologist*, *209*, 978–986.

Boelman, N. T., Rocha, A. V., & Shaver, G. R. (2011). Understanding burn severity sensing in Arctic tundra: Exploring vegetation indices, suboptimal assessment timing and the impact of increasing pixel size. *International Journal of Remote Sensing*, *32*, 7033–7056.

Bond-Lamberty, B., Peckham, S. D., Ahl, D. E., & Gower, S. T. (2007). Fire as the dominant driver of central Canadian boreal forest carbon balance. *Nature*, *450*, 89–92.

Bowden, W. B., Larouche, J. R., Pearce, A. R., Crosby, B. T., Krieger, K., Flinn, M. B., Kampman, J., Gooseff, M. N., Godsey, S. E., Jones, J. B., Abbott, B. W., Jorgenson, M. T., Kling, G. W., Mack, M., Schuur, E. A. G., Baron, A. F., & Rastetter, E. B. (2012). An integrated assessment of the influences of upland thermal-erosional features on landscape structure and function in the foothills of the Brooks Range, Alaska Tenth International. Conference on Permafrost vol *1* (Citeseer) pp 61–66. http://citeseerx.ist.psu.edu/viewdoc/download?doi=10.1.1.296.6775&rep=rep1&type=pdf

Bret-Harte, M. S., Mack, M. C., Shaver, G. R., Huebner, D. C., Johnston, M., Mojica, C. A., Pizano, C., & Reiskind, J. A. (2013). The response of Arctic vegetation and soils following an unusually severe tundra fire. *Philosophical Transactions of the Royal Society B*, *368*, 20120490.

Brookshire, E. N. J., Valett, H. M., & Gerber, S. (2009). Maintenance of terrestrial nutrient loss signatures during in-stream transport. *Ecology*, *90*, 293–299.

Buckeridge, K. M., Banerjee, S., Siciliano, S. D., & Grogan, P. (2013). The seasonal pattern of soil microbial community structure in mesic low arctic tundra. *Soil Biology and Biochemistry*, *65*, 338–347.

Buckeridge, K. M., & Grogan, P. (2010). Deepened snow increases late thaw biogeochemical pulses in mesic low arctic tundra. *Biogeochemistry*, *101*, 105–121.

Buckeridge, K. M., Schaeffer, S. M., & Schimel, J. P. (2016). Vegetation leachate during arctic thaw enhances soil microbial phosphorus. *Ecosystems*, *19*, 477–489.

Burd, K., Tank, S. E., Dion, N., Quinton, W. L., Spence, C., Tanentzap, A. J., & Olefeldt, D. (2018). Seasonal shifts in export of DOC and nutrients from burned and unburned peatland-rich catchments, Northwest Territories, Canada. *Hydrology and Earth System Sciences Discussions*, 1–32.

Bush, R. T., Berke, M. A., & Jacobson, A. D. (2017). Plant Water δD and δ18O of tundra species from west Greenland. *Arctic, Antarctic, and Alpine Research*, *49*, 341–358.

Carey, J. C., Abbott, B. W., & Rocha, A. V. (2019). Plant uptake offsets silica release from a large arctic tundra wildfire. *Earth's Future*, *7*, 1044–1057.

Chen, L., Liu, L., Mao, C., Qin, S., Wang, J., Liu, F., Blagodatsky, S., Yang, G., Zhang, Q., Zhang, D., Yu, J., & Yang, Y. (2018). Nitrogen availability regulates topsoil carbon dynamics after permafrost thaw by altering microbial metabolic efficiency. *Nature Communications*, *9*, 1–11.

Coch, C., Juhls, B., Lamoureux, S. F., Lafrenière, M. J., Fritz, M., Heim, B., & Lantuit, H. (2019). Comparisons of dissolved organic matter and its optical characteristics in small low and high Arctic catchments. *Biogeosciences*, *16*, 4535–4553.

Cory, R. M., Miller, M. P., McKnight, D. M., Guerard, J. J., & Miller, P. L. (2010). Effect of instrument-specific response on the analysis of fulvic acid fluorescence spectra. *Limnology and Oceanography: Methods*, *8*, 67–78.

Craine, J. M., Morrow, C., & Fierer, N. (2007). Microbial nitrogen limitation increases decomposition. *Ecology*, *88*, 2105–2113.

Creed, I. F., Bergström, A.-K., Trick, C. G., Grimm, N. B., Hessen, D. O., Karlsson, J., Kidd, K. A., Kritzberg, E., McKnight, D. M., Freeman, E. C., Senar, O. E., Andersson, A., Ask, J., Berggren, M., Cherif, M., Giesler, R., Hotchkiss, E. R., Kortelainen, P., Palta, M. M., … Weyhenmeyer, G. A. (2018). Global change-driven effects on dissolved organic matter composition: Implications for food webs of northern lakes. *Global Change Biology*, *24*, 3692–3714.

Crump, B. C., Amaral-Zettler, L. A., & Kling, G. W. (2012). Microbial diversity in arctic freshwaters is structured by inoculation of microbes from soils. *ISME Journal*, *6*, 1629–1639.

Darrouzet-Nardi, A., Steltzer, H., Sullivan, P. F., Segal, A., Koltz, A. M., Livensperger, C., Schimel, J. P., & Weintraub, M. N. (2019). Limited effects of early snowmelt on plants, decomposers, and soil nutrients in Arctic tundra soils. *Ecology and Evolution*, *9*, 1820–1844.

DeMarco, J., Mack, M. C., & Bret-Harte, M. S. (2011). The effects of snow, soil microenvironment, and soil organic matter quality on N availability in three Alaskan Arctic plant communities. *Ecosystems*, *14*, 804–817.

Douglas, T. A., Turetsky, M. R., & Koven, C. D. (2020). Increased rainfall stimulates permafrost thaw across a variety of Interior Alaskan boreal ecosystems. *npj Climate and Atmospheric Science*, *3*, 1–7.

Drake, T. W., Tank, S. E., Zhulidov, A. V., Holmes, R. M., Gurtovaya, T., & Spencer, R. G. M. (2018). Increasing alkalinity export from large Russian arctic rivers. *Environmental Science and Technology of Food Industry*, *52*, 8302–8308.

Dupas, R., Minaudo, C., & Abbott, B. W. (2019). Stability of spatial patterns in water chemistry across temperate ecoregions. *Environmental Research Letters*, *14*, 074015.

Ewing, S. A., O'Donnell, J. A., Aiken, G. R., Butler, K., Butman, D., Windham-Myers, L., & Kanevskiy, M. Z. (2015). Long-term anoxia and release of ancient, labile carbon upon thaw of Pleistocene permafrost. *Geophysical Research Letters*, *42*, 2015GL066296.

Fellman, J. B., Spencer, R. G. M., Hernes, P. J., Edwards, R. T., D'Amore, D. V., & Hood, E. (2010). The impact of glacier runoff on the biodegradability and biochemical composition of terrigenous dissolved organic matter in near-shore marine ecosystems. *Marine Chemistry*, *121*, 112–122.

Fisher, R. A., Wieder, W. R., Sanderson, B. M., Koven, C. D., Oleson, K. W., Xu, C., Fisher, J. B., Shi, M., Walker, A. P., & Lawrence, D. M. (2019). Parametric controls on vegetation responses to biogeochemical forcing in the CLM5. *Journal of Advances in Modeling Earth Systems*, *11*, 2879–2895.

Fisher, S. G., Grimm, N. B., Martí, E., Holmes, R. M., & Jones, Jr., J. B. (1998). Material spiraling in stream corridors: A telescoping ecosystem model. *Ecosystems*, *1*, 19–34.

Frei, R. J., Abbott, B. W., Dupas, R., Gu, S., Gruau, G., Thomas, Z., Kolbe, T., Aquilina, L., Labasque, T., Laverman, A., Fovet, O., Moatar, F., & Pinay, G. (2020). Predicting nutrient incontinence in the anthropocene at watershed scales. *Frontiers in Environmental Science*, *7*. https://doi.org/10.3389/fenvs.2019.00200

Frey, K. E., & McClelland, J. W. (2009). Impacts of permafrost degradation on arctic river biogeochemistry. *Hydrological Processes*, *23*, 169–182.

Frey, K. E., McClelland, J. W., Holmes, R. M., & Smith, L. C. (2007). Impacts of climate warming and permafrost thaw on the riverine transport of nitrogen and phosphorus to the Kara Sea. *Journal of Geophysical Research*, *112*. https://doi.org/10.1029/2006JG000369

Frost, G. V., Epstein, H. E., Walker, D. A., Matyshak, G., & Ermokhina, K. (2013). Patterned-ground facilitates shrub expansion in Low Arctic tundra. *Environmental Research Letters*, *8*, 015035.

Gabor, R. S., Baker, A., McKnight, D. M., & Miller, M. P. (2014). *Fluorescence indices and their interpretation aquatic organic matter fluorescence cambridge environmental chemistry series* (pp. 303–338). In A. Baker, D. M. Reynolds, J. Lead, P. G. Coble, &R. G. M. Spencer (Eds.). Cambridge University Press. https://www.cambridge.org/core/books/aquatic-organic-matter-fluorescence/fluorescence-indices-and-their-interpretation/2BB8ADC43278DE03EC24EA2F11B3E94C

Gabor, R. S., Burns, M. A., Lee, R. H., Elg, J. B., Kemper, C. J., Barnard, H. R., & McKnight, D. M. (2015). Influence of leaching solution and catchment location on the fluorescence of water-soluble organic matter. *Environmental Science & Technology*, *49*, 4425–4432.

Gaglioti, B. V., Mann, D. H., Jones, B. M., Pohlman, J. W., Kunz, M. L., & Wooller, M. J. (2014). Radiocarbon age-offsets in an arctic lake reveal the long-term response of permafrost carbon to climate change. *Journal of Geophysical Research. Biogeosciences*, *119*, 1630–1651.

Harms, T. K., Abbott, B. W., & Jones, J. B. (2014). Thermo-erosion gullies increase nitrogen available for hydrologic export. *Biogeochemistry*, *117*, 299–311.

Harms, T. K., & Godsey, S. E. (2017). *Water isotopes of precipitation, surface, and soil waters of the Kuparuk River Basin. Arctic Data Center*. Arctic Data Center. https://arcticdata.io/catalog/view/668ee3cc-f1f8-43ca-b977-339a8eb0aea5

Harms, T. K., & Jones, J. B. (2012). Thaw depth determines reaction and transport of inorganic nitrogen in valley bottom permafrost soils. *Global Change Biology*, *18*, 2958–2968.

Hewitt, R. E., Bennett, A. P., Breen, A. L., Hollingsworth, T. N., Taylor, D. L., Chapin, F. S., & Rupp, T. S. (2015). Getting to the root of the matter: Landscape implications of plant-fungal interactions for tree migration in Alaska. *Landscape Ecology*. https://doi.org/10.1007/s10980-015-0306-1

Higuera, P. E., Chipman, M. L., Barnes, J. L., Urban, M. A., & Hu, F. S. (2011). Variability of tundra fire regimes in Arctic Alaska: Millennial-scale patterns and ecological implications. *Ecological Applications*, *21*, 3211–3226.

Hoffman, F. M., Koven, C. D., Keppel-Aleks, G., Lawrence, D. M., Riley, W. J., Randerson, J. T., Ahlström, A., Abramowitz, G., Baldocchi, D. D., Best, M. J., Bond-Lamberty, B., De Kauwe, M. G., Denning, A. S., Desai, A. R., Eyring, V., Fisher, J. B., Fisher, R. A., Gleckler, P. J., Huang, M., … Koch, D. (2017). *2016 International Land Model Benchmarking (ILAMB) workshop report*. http://www.osti.gov/servlets/purl/1330803/

Högberg, M. N., Briones, M. J. I., Keel, S. G., Metcalfe, D. B., Campbell, C., Midwood, A. J., Thornton, B., Hurry, V., Linder, S., Näsholm, T., & Högberg, P. (2010). Quantification of effects of season and nitrogen supply on tree below-ground carbon transfer to ectomycorrhizal fungi and other soil organisms in a boreal pine forest. *New Phytologist*, *187*, 485–493.

Holloway, J. E., Lewkowicz, A. G., Douglas, T. A., Li, X., Turetsky, M. R., Baltzer, J. L., & Jin, H. (2020). Impact of wildfire on permafrost landscapes: A review of recent advances and future prospects. *Permafrost and Periglacial Processes*, *31*, 371–382.

Holmes, R. M., McClelland, J. W., Peterson, B. J., Tank, S. E., Bulygina, E., Eglinton, T. I., Gordeev, V. V., Gurtovaya, T. Y., Raymond, P. A., Repeta, D. J., Staples, R., Striegl, R. G., Zhulidov, A. V., & Zimov, S. A. (2012). Seasonal and annual fluxes of nutrients and organic matter from large rivers to the arctic ocean and surrounding seas. *Estuaries and Coasts*, *35*, 369–382.

Hu, F. S., Higuera, P. E., Duffy, P., Chipman, M. L., Rocha, A. V., Young, A. M., Kelly, R., & Dietze, M. C. (2015). Arctic tundra fires: natural

variability and responses to climate change. *Frontiers in Ecology and the Environment*, *13*, 369–377.

Hu, F. S., Higuera, P. E., Walsh, J. E., Chapman, W. L., Duffy, P. A., Brubaker, L. B., & Chipman, M. L. (2010). Tundra burning in Alaska: Linkages to climatic change and sea ice retreat. *Journal of Geophysical Research: Biogeosciences*, *115*. https://doi.org/10.1029/2009JG001270

Hugelius, G. (2012). Spatial upscaling using thematic maps: An analysis of uncertainties in permafrost soil carbon estimates. *Global Biogeochemical Cycles*, *26*, n/a-n/a.

Hurrell, J. W., Holland, M. M., Gent, P. R., Ghan, S., Kay, J. E., Kushner, P. J., Lamarque, J.-F., Large, W. G., Lawrence, D., Lindsay, K., Lipscomb, W. H., Long, M. C., Mahowald, N., Marsh, D. R., Neale, R. B., Rasch, P., Vavrus, S., Vertenstein, M., Bader, D., … Marshall, S. (2013). The community earth system model: A framework for collaborative research. *The Bulletin of the American Meteorological Society*, *94*, 1339–1360.

Iwahana, G., Harada, K., Uchida, M., Tsuyuzaki, S., Saito, K., Narita, K., Kushida, K., & Hinzman, L. D. (2016). Geomorphological and geochemistry changes in permafrost after the 2002 tundra wildfire in Kougarok, Seward Peninsula, Alaska. *Journal of Geophysical Research. Earth Surface*, *121*, 2016JF003921.

Jandt, R. R., Miller, E. A., Yokel, D. A., Bret-Harte, M. S., Kolden, C. A., & Mack, M. C. (2012). *Findings of Anaktuvuk river fire recovery study* (pp. 2007–2011). https://www.sciencebase.gov/catalog/item/5a3946c7e4b0d05ee8b407a0

Jiang, Y., Rastetter, E. B., Rocha, A. V., Pearce, A. R., Kwiatkowski, B. L., & Shaver, G. R. (2015). Modeling carbon–nutrient interactions during the early recovery of tundra after fire. *Ecological Applications*, *25*, 1640–1652.

Jiang, Y., Rastetter, E. B., Shaver, G. R., Rocha, A. V., Zhuang, Q., & Kwiatkowski, B. L. (2017). Modeling long-term changes in tundra carbon balance following wildfire, climate change, and potential nutrient addition. *Ecological Applications*, *27*, 105–117.

Jiang, Y., Rocha, A. V., O'Donnell, J. A., Drysdale, J. A., Rastetter, E. B., Shaver, G. R., & Zhuang, Q. (2014). Contrasting soil thermal responses to fire in Alaskan tundra and boreal forest. *Journal of Geophysical Research: Earth Surface*, *120*, 363–378.

Jiang, Y., Rocha, A. V., Rastetter, E. B., Shaver, G. R., Mishra, U., Zhuang, Q., & Kwiatkowski, B. L. (2015). C-N–P interactions control climate driven changes in regional patterns of C storage on the North Slope of Alaska Landscape. *Ecology*. https://doi.org/10.1007/s10980-015-0266-5

Jones, B. M., Breen, A. L., Gaglioti, B. V., Mann, D. H., Rocha, A. V., Grosse, G., Arp, C. D., Kunz, M. L., & Walker, D. A. (2013). Identification of unrecognized tundra fire events on the north slope of Alaska. *Journal of Geophysical Research. Biogeosciences*, *118*, 1334–1344.

Jones, B. M., Grosse, G., Arp, C. D., Miller, E., Liu, L., Hayes, D. J., & Larsen, C. F. (2015). Recent arctic tundra fire initiates widespread thermokarst development. *Scientific Reports*, *5*, 15865.

Jones, B. M., Kolden, C. A., Jandt, R., Abatzoglou, J. T., Urban, F., & Arp, C. D. (2009). Fire behavior, weather, and burn severity of the 2007 Anaktuvuk river tundra fire. *North Slope, Alaska Arctic, Antarctic, and Alpine Research*, *41*, 309–316.

Jones, J. B., Petrone, K. C., Finlay, J. C., Hinzman, L. D., & Bolton, W. R. (2005). Nitrogen loss from watersheds of interior Alaska underlain with discontinuous permafrost. *Geophysical Research Letters*, *32*, L02401.

Jorgenson, M. T., Harden, J., Kanevskiy, M., O'Donnell, J., Wickland, K., Ewing, S., Manies, K., Zhuang, Q., Shur, Y., Striegl, R., & Koch, J. (2013). Reorganization of vegetation, hydrology and soil carbon after permafrost degradation across heterogeneous boreal landscapes. *Environmental Research Letters*, *8*, 035017.

Jorgenson, M. T., & Osterkamp, T. E. (2005). Response of boreal ecosystems to varying modes of permafrost degradation. *Canadian Journal of Forest Research*, *35*, 2100–2111.

Kawahigashi, M., Kaiser, K., Rodionov, A., & Guggenberger, G. (2006). Sorption of dissolved organic matter by mineral soils of the Siberian forest tundra. *Global Change Biology*, *12*, 1868–1877.

Kawahigashi, M., Prokushkin, A., & Sumida, H. (2011). Effect of fire on solute release from organic horizons under larch forest in Central Siberian permafrost terrain. *Geoderma*, *166*, 171–180.

Kelleher, C., Ward, A., Knapp, J. L. A., Blaen, P. J., Kurz, M. J., Drummond, J. D., Zarnetske, J. P., Hannah, D. M., Mendoza-Lera, C., Schmadel, N. M., Datry, T., Lewandowski, J., Milner, A. M., & Krause, S. (2019). Exploring tracer information and model framework trade-offs to improve estimation of stream transient storage processes. *Water Resources Research*, *55*, 3481–3501.

Keller, K., Blum, J. D., & Kling, G. W. (2010). Stream geochemistry as an indicator of increasing permafrost thaw depth in an arctic watershed. *Chemical Geology*, *273*, 76–81.

Kellerman, A. M., Guillemette, F., Podgorski, D. C., Aiken, G. R., Butler, K. D., & Spencer, R. G. M. (2018). Unifying concepts linking dissolved organic matter composition to persistence in aquatic ecosystems. *Environmental Science and Technology of Food Industry*, *52*, 2538–2548.

Kendrick, M. R., Huryn, A. D., Bowden, W. B., Deegan, L. A., Findlay, R. H., Hershey, A. E., Peterson, B. J., Beneš, J. P., & Schuett, E. B. (2018). Linking permafrost thaw to shifting biogeochemistry and food web resources in an arctic river. *Global Change Biology*, *24*, 5738–5750.

Keuper, F., Dorrepaal, E., van Bodegom, P. M., van Logtestijn, R., Venhuizen, G., van Hal, J., & Aerts, R. (2017). Experimentally increased nutrient availability at the permafrost thaw front selectively enhances biomass production of deep-rooting subarctic peatland species. *Global Change Biology*, *23*, 4257–4266.

Keuper, F., Wild, B., Kummu, M., Beer, C., Blume-Werry, G., Fontaine, S., Gavazov, K., Gentsch, N., Guggenberger, G., Hugelius, G., Jalava, M., Koven, C., Krab, E. J., Kuhry, P., Monteux, S., Richter, A., Shahzad, T., Weedon, J. T., & Dorrepaal, E. (2020). Carbon loss from northern circumpolar permafrost soils amplified by rhizosphere priming. *Nature Geoscience*, 1–6.

Kicklighter, D. W., Hayes, D. J., McClelland, J. W., Peterson, B. J., McGuire, A. D., & Melillo, J. M. (2013). Insights and issues with simulating terrestrial DOC loading of Arctic river networks. *Ecological Applications*, *23*, 1817–1836.

Kim, J.-S., Kug, J.-S., Jeong, S.-J., Park, H., & Schaepman-Strub, G. (2020). Extensive fires in southeastern Siberian permafrost linked to preceding Arctic Oscillation. *Science Advances*, *6*, eaax3308.

King, T. V., Neilson, B. T., Overbeck, L. D., & Kane, D. L. (2016). Water temperature controls in low arctic rivers. *Water Resources Research*, *52*, 4358–4376.

King, T. V., Neilson, B. T., & Rasmussen, M. T. (2018). Estimating discharge in low-order rivers with high-resolution aerial imagery. *Water Resources Research*, *54*, 863–878.

Kirdyanov, A., Saurer, M., Siegwolf, R., Knorre, A. A., Prokushkin, A., Churakova (Sidorova), O. V., Fonti, M. V., & Buentgen, U. (2020). Long-term ecological consequences of forest fires in the continuous permafrost zone of Siberia. *Environmental Research Letters*. https://doi.org/10.1088/1748-9326/ab7469

Kling, G. W., Kipphut, G. W., Miller, M. M., & O'Brien W.J. (2000). Integration of lakes and streams in a landscape perspective: The importance of material processing on spatial patterns and temporal coherence. *Freshwater Biology*, *43*, 477–497.

Kokelj, S. V., & Jorgenson, M. T. (2013). Advances in thermokarst research: Recent advances in research investigating thermokarst processes. *Permafrost and Periglacial Processes*, *24*, 108–119.

Kolden, C. A., & Rogan, J. (2013). Mapping wildfire burn severity in the arctic tundra from downsampled MODIS data. *Arctic, Antarctic, and Alpine Research*, *45*, 64–76.

Kou, D., Yang, G., Li, F., Feng, X., Zhang, D., Mao, C., Zhang, Q., Peng, Y., Ji, C., Zhu, Q., Fang, Y., Liu, X., Xu-Ri, L. S., Deng, J., Zheng, X., Fang, J., & Yang, Y. (2020). Progressive nitrogen limitation across

the Tibetan alpine permafrost region. *Nature Communications*, *11*, 3331.

Landhausser, S. M., & Wein, R. W. (1993). Postfire vegetation recovery and tree establishment at the arctic treeline: Climate-change-vegetation-response hypotheses. *Journal of Ecology*, *81*, 665–672.

Larouche, J. R., Abbott, B. W., Bowden, W. B., & Jones, J. B. (2015). The role of watershed characteristics, permafrost thaw, and wildfire on dissolved organic carbon biodegradability and water chemistry in Arctic headwater streams. *Biogeosciences*, *12*, 4221–4233.

Laudon, H., Tetzlaff, D., Soulsby, C., Carey, S., Seibert, J., Buttle, J., Shanley, J., McDonnell, J. J., & McGuire, K. (2013). Change in winter climate will affect dissolved organic carbon and water fluxes in mid-to-high latitude catchments. *Hydrological Processes*, *27*, 700–709.

Lawrence, D. M., Koven, C. D., Swenson, S. C., Riley, W. J., & Slater, A. G. (2015). Permafrost thaw and resulting soil moisture changes regulate projected high-latitude CO_2 and CH_4 emissions. *Environmental Research Letters*, *10*, 094011.

Lawrence, D. M., Oleson, K. W., Flanner, M. G., Thornton, P. E., Swenson, S. C., Lawrence, P. J., Zeng, X., Yang, Z.-L., Levis, S., Sakaguchi, K., Bonan, G. B., & Slater, A. G. (2011). Parameterization improvements and functional and structural advances in Version 4 of the Community Land Model. *Journal of Advances in Modeling Earth Systems*, *3*, M03001.

Lehn, G. O., Jacobson, A. D., Douglas, T. A., McClelland, J. W., Barker, A. J., & Khosh, M. S. (2017). Constraining seasonal active layer dynamics and chemical weathering reactions occurring in North Slope Alaskan watersheds with major ion and isotope ($\delta^{34}S$ SO_4, $\delta^{13}C$ DIC, 87 Sr/ 86 Sr, δ 44/40 Ca, and δ 44/42 Ca) measurements. *Geochimica et Cosmochimica Acta*, *217*, 399–420.

Liu, L., Jafarov, E. E., Schaefer, K. M., Jones, B. M., Zebker, H. A., Williams, C. A., Rogan, J., & Zhang, T. (2014). InSAR detects increase in surface subsidence caused by an Arctic tundra fire. *Geophysical Research Letters*, *41*, 3906–3913.

Loranty, M. M., Abbott, B. W., Blok, D., Douglas, T. A., Epstein, H. E., Forbes, B. C., Jones, B. M., Kholodov, A. L., Kropp, H., Malhotra, A., Mamet, S. D., Myers-Smith, I. H., Natali, S. M., O'Donnell, J. A., Phoenix, G. K., Rocha, A. V., Sonnentag, O., Tape, K. D., & Walker, D. A. (2018). Reviews and syntheses: Changing ecosystem influences on soil thermal regimes in northern high-latitude permafrost regions. *Biogeosciences*, *15*, 5287–5313.

Loranty, M. M., Liberman-Cribbin, W., Berner, L. T., Natali, S. M., Goetz, S. J., Alexander, H. D., & Kholodov, A. L. (2016). Spatial variation in vegetation productivity trends, fire disturbance, and soil carbon across arctic-boreal permafrost ecosystems. *Environmental Research Letters*, *11*, 095008.

Lovett, G. M., Goodale, C. L., Ollinger, S. V., Fuss, C. B., Ouimette, A. P., & Likens, G. E. (2018). Nutrient retention during ecosystem succession: A revised conceptual model. *Frontiers in Ecology and the Environment*, *16*, 532–538.

Ludwig, S. M., Alexander, H. D., Kielland, K., Mann, P. J., Natali, S. M., & Ruess, R. W. (2018). Fire severity effects on soil carbon and nutrients and microbial processes in a Siberian larch forest. *Global Change Biology*, *24*, 5841–5852.

Lyon, S. W., Nathanson, M., Spans, A., Grabs, T., Laudon, H., Temnerud, J., Bishop, K. H., & Seibert, J. (2012). Specific discharge variability in a boreal landscape. *Water Resources Research*, *48*, W08506.

Mack, M. C., Bret-Harte, M. S., Hollingsworth, T. N., Jandt, R. R., Schuur, E. A. G., Shaver, G. R., & Verbyla, D. L. (2011). Carbon loss from an unprecedented Arctic tundra wildfire. *Nature*, *475*, 489–492.

Mack, M. C., Schuur, E. A. G., Bret-Harte, M. S., Shaver, G. R., & Chapin, F. S. (2004). Ecosystem carbon storage in arctic tundra reduced by long-term nutrient fertilization. *Nature*, *431*, 440–443.

Mack, M. C., Treseder, K. K., Manies, K. L., Harden, J. W., Schuur, E. A. G., Vogel, J. G., Randerson, J. T., & Chapin, F. S. (2008). Recovery of aboveground plant biomass and productivity after fire in mesic and dry black spruce forests of interior Alaska. *Ecosystems*, *11*, 209–225.

MacLean, R., Oswood, M. W., Irons, J. G., & McDowell, W. H. (1999). The effect of permafrost on stream biogeochemistry: A case study of two streams in the Alaskan (U.S.A.) taiga. *Biogeochemistry*, *47*, 239–267.

Malone, E. T., Abbott, B. W., Klaar, M. J., Kidd, C., Sebilo, M., Milner, A. M., & Pinay, G. (2018). Decline in ecosystem $\delta^{13}C$ and mid-successional nitrogen loss in a two-century postglacial chronosequence. *Ecosystems*, *21*, 1659–1675.

Mann, P. J., Spencer, R. G. M., Hernes, P. J., Six, J., Aiken, G. R., Tank, S. E., McClelland, J. W., Butler, K. D., Dyda, R. Y., & Holmes, R. M. (2016). Pan-Arctic trends in terrestrial dissolved organic matter from optical measurements. *Frontiers Earth Science*, *4*. https://doi.org/10.3389/feart.2016.00025/abstract

McClelland, J. W., Holmes, R. M., Dunton, K. H., & Macdonald, R. W. (2012). The arctic ocean estuary. *Estuaries and Coasts*, *35*, 353–368.

McClelland, J. W., Stieglitz, M., Pan, F., Holmes, R. M., & Peterson, B. J. (2007). Recent changes in nitrate and dissolved organic carbon export from the upper Kuparuk River, North Slope, Alaska. *Journal of Geophysical Research*, *112*. https://doi.org/10.1029/2006JG000371

McClelland, J. W., Townsend-Small, A., Holmes, R. M., Pan, F., Stieglitz, M., Khosh, M., & Peterson, B. J. (2014). River export of nutrients and organic matter from the North Slope of Alaska to the Beaufort Sea. *Water Resources Research*, *50*, 1823–1839.

McGuire, A. D., Lawrence, D. M., Koven, C., Clein, J. S., Burke, E., Chen, G., Jafarov, E., MacDougall, A. H., Marchenko, S., Nicolsky, D., Peng, S., Rinke, A., Ciais, P., Gouttevin, I., Hayes, D. J., Ji, D., Krinner, G., Moore, J. C., Romanovsky, V., … Zhuang, Q. (2018). Dependence of the evolution of carbon dynamics in the northern permafrost region on the trajectory of climate change. *Proceedings of the National Academy of Sciences of the United States of America*, *115*, 3882–3887.

McGuire, K. J., Torgersen, C. E., Likens, G. E., Buso, D. C., Lowe, W. H., & Bailey, S. W. (2014). Network analysis reveals multiscale controls on streamwater chemistry. *Proceedings of the National Academy of Sciences of the United States of America*, *111*, 7030–7035.

McKnight, D. M., Boyer, E. W., Westerhoff, P. K., Doran, P. T., Kulbe, T., & Andersen, D. T. (2001). Spectrofluorometric characterization of dissolved organic matter for indication of precursor organic material and aromaticity. *Limnology and Oceanography*, *46*, 38–48.

McLaren, J. R., Darrouzet-Nardi, A., Weintraub, M. N., & Gough, L. (2017). Seasonal patterns of soil nitrogen availability in moist acidic tundra Arctic. *Science*. https://doi.org/10.1139/AS-2017-0014

Melle, C., Wallenstein, M., Darrouzet-Nardi, A., & Weintraub, M. N. (2015). Microbial activity is not always limited by nitrogen in Arctic tundra soils. *Soil Biology and Biochemistry*, *90*, 52–61.

Metcalfe, D. B., Hermans, T. D. G., Ahlstrand, J., Becker, M., Berggren, M., Björk, R. G., Björkman, M. P., Blok, D., Chaudhary, N., Chisholm, C., Classen, A. T., Hasselquist, N. J., Jonsson, M., Kristensen, J. A., Kumordzi, B. B., Lee, H., Mayor, J. R., Prevéy, J., Pantazatou, K., … Abdi, A. M. (2018). Patchy field sampling biases understanding of climate change impacts across the Arctic. *Nature Ecology & Evolution*, *1*.

Minaudo, C., Dupas, R., Gascuel-Odoux, C., Fovet, O., Mellander, P.-E., Jordan, P., Shore, M., & Moatar, F. (2017). Nonlinear empirical modeling to estimate phosphorus exports using continuous records of turbidity and discharge: P exports from turbidity and discharge. *Water Resources Research*, *53*, 7590–7606.

Mollenhauer, G., Winterfeld, M., Hefter, J., Grotheer, H., Kattein, L., & Ransby, D. (2019). No evidence for 20th century acceleration in fossil carbon supply to the ocean from thawing permafrost in the Lena River catchment. EPIC3Goldschmidt Conference, Barcelona, 2019-08-18-2019-08-23 Goldschmidt Conference (Barcelona). https://epic.awi.de/id/eprint/50144/

Mu, C. C., Abbott, B. W., Wu, X. D., Zhao, Q., Wang, H. J., Su, H., Wang, S. F., Gao, T. G., Guo, H., Peng, X. Q., & Zhang, T. J. (2017). Thaw depth determines dissolved organic carbon concentration and biodegradability on the northern Qinghai-Tibetan Plateau. *Geophysical Research Letters*, 2017GL075067.

Myers-Smith, I. H., Elmendorf, S. C., Beck, P. S. A., Wilmking, M., Hallinger, M., Blok, D., Tape, K. D., Rayback, S. A., Macias-Fauria, M., Forbes, B. C., Speed, J. D. M., Boulanger-Lapointe, N., Rixen, C., Lévesque, E., Schmidt, N. M., Baittinger, C., Trant, A. J., Hermanutz, L., Collier, L. S. … Vellend, M. (2015). Climate sensitivity of shrub growth across the tundra biome. *Nature Climate Change*, *5*, nclimate2697.

Myers-Smith, I. H., Forbes, B. C., Wilmking, M., Hallinger, M., Lantz, T., Blok, D., Tape, K. D., Macias-Fauria, M., Sass-Klaassen, U., Lévesque, E., Boudreau, S., Ropars, P., Hermanutz, L., Trant, A., Collier, L. S., Weijers, S., Rozema, J., Rayback, S. A., Schmidt, N. M., … Hik, D. S. (2011). Shrub expansion in tundra ecosystems: Dynamics, impacts and research priorities. *Environmental Research Letters*, *6*, 045509.

Neilson, B. T., Cardenas, M. B., O'Connor, M. T., Rasmussen, M. T., King, T. V., & Kling, G. W. (2018). Groundwater flow and exchange across the land surface explain carbon export patterns in continuous permafrost watersheds. *Geophysical Research Letters*, *45*, 7596–7605.

Neumann, R. B., Moorberg, C. J., Lundquist, J. D., Turner, J. C., Waldrop, M. P., McFarland, J. W., Euskirchen, E. S., Edgar, C. W., & Turetsky, M. R. (2019). Warming effects of spring rainfall increase methane emissions from thawing permafrost. *Geophysical Research Letters*, *46*, 1393–1401.

O'Donnell, J. A., Aiken, G. R., Butler, K. D., Guillemette, F., Podgorski, D. C., & Spencer, R. G. M. (2016). DOM composition and transformation in boreal forest soils: The effects of temperature and organic-horizon decomposition state. *Journal of Geophysical Research: Biogeosciences*, *121*, 2016JG003431.

O'Donnell, J. A., Aiken, G. R., Swanson, D. K., Panda, S., Butler, K. D. Baltensperger, A. P. (2016). Dissolved organic matter composition of Arctic rivers: Linking permafrost and parent material to riverine carbon. *Global Biogeochemical Cycles*.

O'Donnell, J. A., Harden, J. W., Manies, K. L., Jorgenson, M. T., Kanevskiy, M., & Xu, X. (2013). *Soil data from fire and permafrost-thaw chronosequences in upland* Picea mariana *stands near Hess Creek and Tok, interior Alaska* (vol 2013–1045). U.S. Geological Survey. http://pubs.er.usgs.gov/publication/ofr20131045

Oberbauer, S. F., Sionit, N., Hastings, S. J., & Oechel, W. C. (1986). Effects of CO_2 enrichment and nutrition on growth, photosynthesis, and nutrient concentration of Alaskan tundra plant species. *Canadian Journal of Botany*, *64*, 2993–2998.

Olefeldt, D., Goswami, S., Grosse, G., Hayes, D., Hugelius, G., Kuhry, P., McGuire, A. D., Romanovsky, V. E., Sannel, A. B. K., Schuur, E. A. G., & Turetsky, M. R. (2016). Circumpolar distribution and carbon storage of thermokarst landscapes. *Nature Communications*, *7*, 13043.

Parham, L. M., Prokushkin, A. S., Pokrovsky, O. S., Titov, S. V., Grekova, E., Shirokova, L. S., & McDowell, W. H. (2013). Permafrost and fire as regulators of stream chemistry in basins of the Central Siberian Plateau. *Biogeochemistry*, *116*, 55–68.

Pearce, A. R., Rastetter, E. B., Kwiatkowski, B. L., Bowden, W. B., Mack, M. C., & Jiang, Y. (2014). Recovery of arctic tundra from thermal erosion disturbance is constrained by nutrient accumulation: A modeling analysis. *Ecological Applications*. https://doi.org/10.1890/14-1323.1

Petrone, K. C., Jones, J. B., Hinzman, L. D., & Boone, R. D. (2006). Seasonal export of carbon, nitrogen, and major solutes from Alaskan catchments with discontinuous permafrost. *Journal of Geophysical Research*, *111*. https://doi.org/10.1029/2005JG000055

Pinay, G., Peiffer, S., De Dreuzy, J.-R., Krause, S., Hannah, D. M., Fleckenstein, J. H., Sebilo, M., Bishop, K., & Hubert-Moy, L. (2015). Upscaling nitrogen removal capacity from local hotspots to low stream orders' drainage basins. *Ecosystems*, *18*, 1101–1120.

Porter, C., Morin, P., Howat, I., Noh, M.-J., Bates, B., Peterman, K., Keesey, S., Schlenk, M., Gardiner, J., Tomko, K., Willis, M., Kelleher, C., Cloutier, M., Husby, E., Foga, S., Nakamura, H., Platson, M., Wethington, M., Williamson, C., … Bojesen, M. (2018). ArcticDEM. https://dataverse.harvard.edu/citation?persistentId=doi:10.7910/DVN/OHHUKH

R Core Team. (2018). *R: A language and environment for statistical computing*. R Foundation for Statistical Computing. https://www.R-project.org/

Racine, C., Jandt, R., Meyers, C., & Dennis, J. (2004). Tundra fire and vegetation change along a hillslope on the Seward Peninsula, Alaska, U.S.A. *Arctic, Antarctic, and Alpine Research*, *36*, 1–10.

Rastetter, E. B., Kling, G. W., Shaver, G. R., Crump, B. C., Gough, L., & Griffin, K. L. (2020). Ecosystem recovery from disturbance is constrained by N cycle openness, vegetation-soil n distribution, form of N losses, and the balance between vegetation and soil-microbial processes. *Ecosystems*. https://doi.org/10.1007/s10021-020-00542-3

Raymond, P. A., McClelland, J. W., Holmes, R. M., Zhulidov, A. V., Mull, K., Peterson, B. J., Striegl, R. G., Aiken, G. R., & Gurtovaya, T. Y. (2007). Flux and age of dissolved organic carbon exported to the Arctic Ocean: A carbon isotopic study of the five largest arctic rivers. *Global Biogeochemical Cycles*, *21*, GB4011.

Rey, D. M., Walvoord, M. A., Minsley, B. J., Ebel, B. A., Voss, C. I., & Singha, K. (2020). Wildfire initiated talik development exceeds current thaw projections: Observations and models from Alaska's continuous permafrost zone. *Geophysical Research Letters*, e2020GL087565.

Reyes, F. R., & Lougheed, V. L. (2015). Rapid nutrient release from permafrost thaw in arctic aquatic ecosystems. *Arctic, Antarctic, and Alpine Research*, *47*, 35–48.

Rhoades, C., Oskarsson, H., Binkley, D., & Stottlemyer, B. (2001). Alder (*Alnus crispa*) effects on soils in ecosystems of the Agashashok River valley, northwest Alaska. *Écoscience*, *8*, 89–95.

Rocha, A. V., Loranty, M. M., Higuera, P. E., Mack, M. C., Hu, F. S., Jones, B. M., Breen, A. L., Rastetter, E. B., Goetz, S. J., & Shaver, G. R. (2012). The footprint of Alaskan tundra fires during the past half-century: Implications for surface properties and radiative forcing. *Environmental Research Letters.*, *7*, 044039.

Rocha, A. V., & Shaver, G. R. (2011a). Burn severity influences postfire CO_2 exchange in arctic tundra. *Ecological Applications*, *21*, 477–489.

Rocha, A. V., & Shaver, G. R. (2011b). Postfire energy exchange in arctic tundra: The importance and climatic implications of burn severity. *Global Change Biology*, *17*, 2831–2841.

Rodríguez-Cardona, B. M., Coble, A. A., Wymore, A. S., Kolosov, R., Podgorski, D. C., Zito, P., Spencer, R. G. M., Prokushkin, A. S., & McDowell, W. H. (2020). Wildfires lead to decreased carbon and increased nitrogen concentrations in upland arctic streams. *Scientific Reports*, *10*, 8722.

Ruess, R. W., Anderson, M. D., McFarland, J. M., Kielland, K., Olson, K., & Taylor, D. L. (2013). Ecosystem-level consequences of symbiont partnerships in an N-fixing shrub from interior Alaskan floodplains. *Ecological Monographs*, *83*, 177–194.

Salmon, V. G., Schädel, C., Bracho, R., Pegoraro, E., Celis, G., Mauritz, M., Mack, M. C., & Schuur, E. A. G. (2018). Adding depth to our understanding of nitrogen dynamics in permafrost soils. *Journal of Geophysical Research: Biogeosciences*, *123*, 2497–2512.

Schuur, E. A. G., McGuire, A. D., Schädel, C., Grosse, G., Harden, J. W., Hayes, D. J., Hugelius, G., Koven, C. D., Kuhry, P., Lawrence, D. M., Natali, S. M., Olefeldt, D., Romanovsky, V. E., Schaefer, K., Turetsky, M. R., Treat, C. C., & Vonk, J. E. (2015). Climate change and the permafrost carbon feedback. *Nature*, *520*, 171–179.

Shogren, A. J., Zarnetske, J. P., Abbott, B. W., Iannucci, F., & Bowden, W. B. (2020). We cannot shrug off the shoulder seasons: Addressing knowledge and data gaps in an Arctic Headwater. *Environmental Letters Reseach*. https://doi.org/10.1088/1748-9326/ab9d3c

Shogren, A. J., Zarnetske, J. P., Abbott, B. W., Iannucci, F., Frei, R. J., Griffin, N. A., & Bowden, W. B. (2019). Revealing biogeochemical

signatures of arctic landscapes with river chemistry. *Science Reports*, *9*, 1–11.

Shur, Y. L., & Jorgenson, M. T. (2007). Patterns of permafrost formation and degradation in relation to climate and ecosystems. *Permafrost and Periglacial Processes*, *18*, 7–19.

Sigman, D. M., Casciotti, K. L., Andreani, M., Barford, C., Galanter, M., & Böhlke, J. K. (2001). A bacterial method for the nitrogen isotopic analysis of nitrate in seawater and freshwater. *Analytical Chemistry*, *73*, 4145–4153.

Slavik, K., Peterson, B. J., Deegan, L. A., Bowden, W. B., Hershey, A. E., & Hobbie, J. E. (2004). Long-term responses of the kuparuk river ecosystem to phosphorus fertilization. *Ecology*, *85*, 939–954.

Strauss, J., Schirrmeister, L., Grosse, G., Fortier, D., Hugelius, G., Knoblauch, C., Romanovsky, V., Schädel, C., Schneider von Deimling, T., Schuur, E. A. G., Shmelev, D., Ulrich, M., & Veremeeva, A. (2017). Deep Yedoma permafrost: A synthesis of depositional characteristics and carbon vulnerability. *Earth-Science Reviews*, *172*, 75–86.

Striegl, R. G., Aiken, G. R., Dornblaser, M. M., Raymond, P. A., & Wickland, K. P. (2005). A decrease in discharge-normalized DOC export by the Yukon River during summer through autumn. *Geophysical Research Letters*, *32*. https://doi.org/10.1029/2005GL024413

Sturm, M., Racine, C., & Tape, K. (2001). Climate change: Increasing shrub abundance in the Arctic. *Nature*, *411*, 546–547.

Sturm, M., Schimel, J., Michaelson, G., Welker, J. M., Oberbauer, S. F., Liston, G. E., Fahnestock, J., & Romanovsky, V. E. (2005). Winter biological processes could help convert arctic tundra to shrubland. *BioScience*, *55*, 17–26.

Tank, S. E., Striegl, R. G., McClelland, J. W., & Kokelj, S. V. (2016). Multi-decadal increases in dissolved organic carbon and alkalinity flux from the Mackenzie drainage basin to the Arctic Ocean. *Environmental Research Letters*, *11*, 054015.

Tank, S. E., Vonk, J. E., Walvoord, M. A., McClelland, J. W., Laurion, I., & Abbott, B. W. (2020). Landscape matters: Predicting the biogeochemical effects of permafrost thaw on aquatic networks with a state factor approach. *Permafrost and Periglacial Processes*. https://doi.org/10.1002/ppp.2057

Temnerud, J., & Bishop, K. (2005). Spatial variation of streamwater chemistry in two swedish boreal catchments? Implications for environmental assessment. *Environmental Science & Technology*, *39*, 1463–1469.

Tierney, J. A., Hedin, L. O., & Wurzburger, N. (2019). Nitrogen fixation does not balance fire-induced nitrogen losses in longleaf pine savannas. *Ecology*, *100*, e02735.

Toohey, R. C., Herman-Mercer, N. M., Schuster, P. F., Mutter, E. A., & Koch, J. C. (2016). Multidecadal increases in the Yukon River Basin of chemical fluxes as indicators of changing flowpaths, groundwater, and permafrost. *Geophysical Research Letters*, *43*, 12120–12130.

Toolik Environmental Data Center Team. (2019). *Meterological monitoring program at Toolik, Alaska, Toolik Field Station*. Institute of Arctic Biology, University of Alaska Fairbanks. https://toolik.alaska.edu/edc/

Treat, C. C., Wollheim, W. M., Varner, R. K., & Bowden, W. B. (2016). Longer thaw seasons increase nitrogen availability for leaching during fall in tundra soils. *Environmental Research Letters*, *11*, 064013.

Turetsky, M. R., Abbott, B. W., Jones, M. C., Anthony, K. W., Olefeldt, D., Schuur, E. A. G., Grosse, G., Kuhry, P., Hugelius, G., Koven, C., Lawrence, D. M., Gibson, C., Sannel, A. B. K., & McGuire, A. D. (2020). Carbon release through abrupt permafrost thaw. *Nature Geoscience*, *13*, 138–143.

Turetsky, M. R., Abbott, B. W., Jones, M. C., Anthony, K. W., Olefeldt, D., Schuur, E. A. G., Koven, C., McGuire, A. D., Grosse, G., Kuhry, P., Hugelius, G., Lawrence, D. M., Gibson, C., & Sannel, A. B. K. (2019). Permafrost collapse is accelerating carbon release. *Nature*, *569*, 32.

Vancoppenolle, M., Bopp, L., Madec, G., Dunne, J., Ilyina, T., Halloran, P. R., & Steiner, N. (2013). Future Arctic Ocean primary productivity from CMIP5 simulations: Uncertain outcome, but consistent mechanisms: Future arctic ocean primary productivity. *Global Biogeochemical Cycles*, *27*, 605–619.

Viereck, L. A., Werdin-Pfisterer, N. R., Adams, P. C., & Yoshikawa, K. (2008). Effect of wildfire and fireline construction on the annual depth of thaw in a black spruce permafrost forest in interior Alaska: A 36-year record of recovery. In D. L. Kane & K. M. Hinkel (Eds.). *Proceedings of the ninth international conference on permafrost* (pp. 1845–1850). June 29-July 3, 2008. https://www.fs.usda.gov/treesearch/pubs/all/32468

Vitousek, P. M., & Reiners, W. A. (1975). Ecosystem succession and nutrient retention: A hypothesis. *BioScience*, *25*, 376–381.

Voigt, C., Marushchak, M. E., Abbott, B. W., Biasi, C., Elberling, B., Siciliano, S. D., Sonnentag, O., Stewart, K. J., Yang, Y., & Martikainen, P. J. (2020). Nitrous oxide emissions from permafrost-affected soils. *Nature Reviews Earth & Environment*, 1–15.

Vonk, J. E., Tank, S. E., Bowden, W. B., Laurion, I., Vincent, W. F., Alekseychik, P., Amyot, M., Billet, M. F., Canário, J., Cory, R. M., Deshpande, B. N., Helbig, M., Jammet, M., Karlsson, J., Larouche, J., MacMillan, G., Rautio, M., Walter Anthony, K. M., & Wickland, K. P. (2015). Reviews and syntheses: Effects of permafrost thaw on Arctic aquatic ecosystems. *Biogeosciences*, *12*, 7129–7167.

Walker, M. D., Wahren, C. H., Hollister, R. D., Henry, G. H., Ahlquist, L. E., Alatalo, J. M., Bret-Harte, M. S., Calef, M. P., Callaghan, T. V., Carroll, A. B., Epstein, H. E., Jónsdóttir, I. S., Klein, J. A., Magnússon, B., Molau, U., Oberbauer, S. F., Rewa, S. P., Robinson, C. H., Shaver, G. R., … Wookey, P. A. (2006). Plant community responses to experimental warming across the tundra biome. *Proceedings of the National Academy of Sciences of the United States of America*, *103*, 1342–1346.

Walker, X. J., Baltzer, J. L., Cumming, S. G., Day, N. J., Ebert, C., Goetz, S., Johnstone, J. F., Potter, S., Rogers, B. M., Schuur, E. A. G., Turetsky, M. R., & Mack, M. C. (2019). Increasing wildfires threaten historic carbon sink of boreal forest soils. *Nature*, *572*, 520–523.

Walvoord, M. A., & Kurylyk, B. L. (2016). Hydrologic impacts of thawing permafrost – A review. *Vadose Zone Journal*, *15*, vzj2016.01.0010.

Wang, J.-J., Lafrenière, M. J., Lamoureux, S. F., Simpson, A. J., Gélinas, Y., & Simpson, M. J. (2018). Differences in riverine and pond water dissolved organic matter composition and sources in canadian high arctic watersheds affected by active layer detachments. *Environmental Science and Technology of Food Industry*, *52*, 1062–1071.

Wauthy, M., Rautio, M., Christoffersen, K. S., Forsström, L., Laurion, I., Mariash, H. L., Peura, S., & Vincent, W. F. (2018). Increasing dominance of terrigenous organic matter in circumpolar freshwaters due to permafrost thaw. *Limnology and Oceanography*, *1–13*.

Wein, R. W., & Bliss, L. C. (1973). Changes in arctic eriophorum tussock communities following fire. *Ecology*, *54*, 845–852.

Weishaar, J. L., Aiken, G. R., Bergamaschi, B. A., Fram, M. S., Fujii, R., & Mopper, K. (2003). Evaluation of specific ultraviolet absorbance as an indicator of the chemical composition and reactivity of dissolved organic carbon. *Environmental Science & Technology*, *37*, 4702–4708.

Weiss, M., Hobbie, S. E., & Gettel, G. M. (2005). Contrasting responses of nitrogen-fixation in arctic lichens to experimental and ambient nitrogen and phosphorus availability. *Arctic, Antarctic, and Alpine Research*, *37*, 396–401.

Wickham, H., Chang, W., Henry, L., Pedersen, T. L., Takahashi, K., Wilke, C., Woo, K., Yutani, H., Dunnington, D., & RStudio. (2020). ggplot2: Create elegant data visualisations using the grammar of graphics. https://CRAN.R-project.org/package=ggplot2

Wickland, K. P., Neff, J. C., & Aiken, G. R. (2007). Dissolved organic carbon in Alaskan boreal forest: Sources. *Chemical Characteristics, and Biodegradability Ecosystems*, *10*, 1323–1340.

Wickland, K. P., Waldrop, M. P., Aiken, G. R., Koch, J. C., Jorgenson, M. T., & Striegl, R. G. (2018). Dissolved organic carbon and nitrogen release from boreal Holocene permafrost and seasonally frozen soils of Alaska. *Environmental Research Letters*, *13*, 065011.

Wieder, W. R., Cleveland, C. C., Smith, W. K., & Todd-Brown, K. (2015). Future productivity and carbon storage limited by terrestrial nutrient availability. *Nature Geoscience*, *8*, 441–444.

Wieder, W. R., Lawrence, D. M., Fisher, R. A., Bonan, G. B., Cheng, S. J., Goodale, C. L., Grandy, A. S., Koven, C. D., Lombardozzi, D. L., Oleson, K. W., & Thomas, R. Q. (2019). Beyond static benchmarking: Using experimental manipulations to evaluate land model assumptions. *Global Biogeochemical Cycles*, *33*, 1289–1309.

Wild, B., Andersson, A., Bröder, L., Vonk, J., Hugelius, G., McClelland, J. W., Song, W., Raymond, P. A., & Gustafsson, Ö. (2019). Rivers across the Siberian Arctic unearth the patterns of carbon release from thawing permafrost. *Proceedings of the National Academy of Sciences of the United States of America*, *116*, 10280–10285.

Wologo, E., Shakil, S., Zolkos, S., Textor, S., Ewing, S., Klassen, J., Spencer, R. G. M., Podgorski, D. C., Tank, S. E., Baker, M. A., O'Donnell, J. A., Wickland, K. P., Foks, S. S. W., Zarnetske, J. P., Lee-Cullin, J., Liu, F., Yang, Y., Kortelainen, P., Kolehmainen, J., … Abbott, B. W. (2020). Stream dissolved organic matter in permafrost regions shows surprising compositional similarities but negative priming and nutrient effects. *Global Biogeochemical Cycles*, e2020GB006719.

Wright, K. S., & Rocha, A. V. (2018). A test of functional convergence in carbon fluxes from coupled C and N cycles in Arctic tundra. *Ecological Modelling*, *383*, 31–40.

Wymore, A. S., Leon, M. C., Shanley, J. B., & McDowell, W. H. (2019). Hysteretic response of solutes and turbidity at the event scale across forested tropical montane watersheds. *Frontiers Earth Science*, *7*. https://doi.org/10.3389/feart.2019.00126/full

Yoshikawa, K., Bolton, W. R., Romanovsky, V. E., Fukuda, M., & Hinzman, L. D. (2002). Impacts of wildfire on the permafrost in the boreal forests of Interior Alaska. *Journal of Geophysical Research: Atmospheres*, *107*, FFR4-1–FFR4-14.

Zamin, T. J., & Grogan, P. (2012). Birch shrub growth in the low Arctic: the relative importance of experimental warming, enhanced nutrient availability, snow depth and caribou exclusion. *Environmental Research Letters*, *7*, 034027.

Zarnetske, J. P., Bouda, M., Abbott, B. W., Saiers, J., & Raymond, P. A. (2018). Generality of hydrologic transport limitation of watershed organic carbon flux across ecoregions of the United States. *Geophysical Research Letters*, *45*, 11702–11711.

Zimov, N. S., Zimov, S. A., Zimova, A. E., Zimova, G. M., Chuprynin, V. I., & Chapin, F. S. (2009). Carbon storage in permafrost and soils of the mammoth tundra-steppe biome: Role in the global carbon budget. Carbon storage of the mammoth steppe. *Geophysical Research Letters*, *36*. https://doi.org/10.1029/2008GL036332

Zolkos, S., & Tank, S. E. (2020). Experimental evidence that permafrost thaw history and mineral composition shape abiotic carbon cycling in thermokarst-affected stream networks. *Frontiers Earth Science*, *8*, 152.

SUPPORTING INFORMATION

Additional supporting information may be found online in the Supporting Information section.

How to cite this article: Abbott BW, Rocha AV, Shogren A, et al. Tundra wildfire triggers sustained lateral nutrient loss in Alaskan Arctic. *Glob Change Biol*. 2021;00:1–23. https://doi.org/10.1111/gcb.15507